

Rapid weed adaptation and range expansion in response to agriculture over the last two centuries

Short title: Weed adaptation to modern agriculture

Julia Kreiner^{*1,2}, Sergio M. Latorre^{3,4}, Hernán A. Burbano^{3,4}, John R. Stinchcombe⁵, Sarah P. Otto^{2,6}, Detlef Weigel⁴, & Stephen Wright⁵

Affiliations:

¹*Department of Botany, University of British Columbia, Vancouver, Canada;*

²*Biodiversity Research Centre, University of British Columbia, Vancouver, Canada;*

³*Centre for Life's Origins and Evolution, Department of Genetics, Evolution and Environment, University College London, London, UK;*

⁴*Department of Molecular Biology, Max Planck Institute for Biology Tübingen, Tübingen, Germany;*

⁵*Department of Ecology and Evolutionary Biology, University of Toronto, Toronto, ON, Canada;*

⁶*Department of Zoology, University of British Columbia, Vancouver, Canada;*

*Corresponding author email: julia.kreiner@ubc.ca

Abstract

North America has seen a massive increase in cropland use since 1800, accompanied more recently by the intensification of agricultural practices. Through genome analysis of present-day and historical samples spanning environments over the last two centuries, we studied the impact of these changes in farming on the extent and tempo of evolution in the native common waterhemp (*Amaranthus tuberculatus*), a now pervasive agricultural weed. Modern agriculture has imposed strengths of selection rarely observed in the wild, with striking shifts in allele frequency trajectories since agricultural intensification in the 1960s. An evolutionary response to this extreme selection was facilitated by a concurrent human-mediated range shift. By reshaping genome-wide diversity and variation for fitness, agriculture has driven the success of this weed in the 21st-century.

One Sentence Summary

Modern agriculture has dramatically shaped the evolution of a native plant into an agricultural weed through imposing strengths of selection rarely observed in the wild.

Main text

Agricultural practices across North America have rapidly intensified over the last two centuries, through cropland expansion (1), habitat homogenization (2), and increased chemical inputs (3, 4). Since the beginning of the 1800s, cropland usage has expanded from 8 million to 200 million hectares in Canada and the United States alone (1). Since the mid 1900's, development of new crop varieties—including high-yield and herbicide-resistant wheat, corn, and soy (5, 6)—have greatly improved the efficiency of food production in all farming sectors. Combined with increased reliance on pesticides, fertilizers, irrigation, and large-scale mechanization, this transformation is oft-referenced as the agricultural “Green Revolution” (7–9). For pesticides, however, their effectiveness has been limited by the evolution of resistance across numerous pest species (10–13). While technological innovation for efficient food production has risen with increasing global food demands, the concomitant conversion of our landscape has become one of the foremost drivers of global biodiversity loss (14).

Species that have managed to survive, and even thrive, in the face of such extreme environmental change provide remarkable examples of rapid adaptation on contemporary timescales and illustrate the evolutionary consequences of anthropogenic impacts. One such species is common waterhemp (*Amaranthus tuberculatus*), which is native to North America and persists in large part in natural, riparian habitats (15, 16), providing a unique opportunity to investigate the timescale and extent of contemporary agricultural adaptation in this prevalent weed. The genetic changes underlying weediness are particularly important to understand in *A. tuberculatus*, as it has recently become one of the most problematic agricultural weeds in North America due to widespread adaptation to herbicides, persistence in fields across seasons, and strong competitive ability with both soy and corn (17, 18). Determining how much of waterhemp's success in agricultural environments has been driven by either newly arisen mutations, genetic variants predating the onset of environmental change (19, 20), or migration across the range (21), as well as their interactions (e.g. (22, 23)), will inform on the temporal and spatial scales at which contemporary adaptation occurs and management strategies should be employed.

To understand how changing agricultural practices have shaped the success of a ubiquitous weed, we analyze genomic data from contemporary paired natural and agricultural populations alongside historical herbarium samples collected from 1828 until 2011 (**Fig 1**). With this design, we identify agriculturally adaptive alleles—those that are consistently higher in frequency in agricultural than in geographically close natural sites which constitute contrasts in selective pressures, track their frequency across nearly two centuries, and link the tempo of weed adaptation to demographic changes and key cultural shifts in modern agriculture.

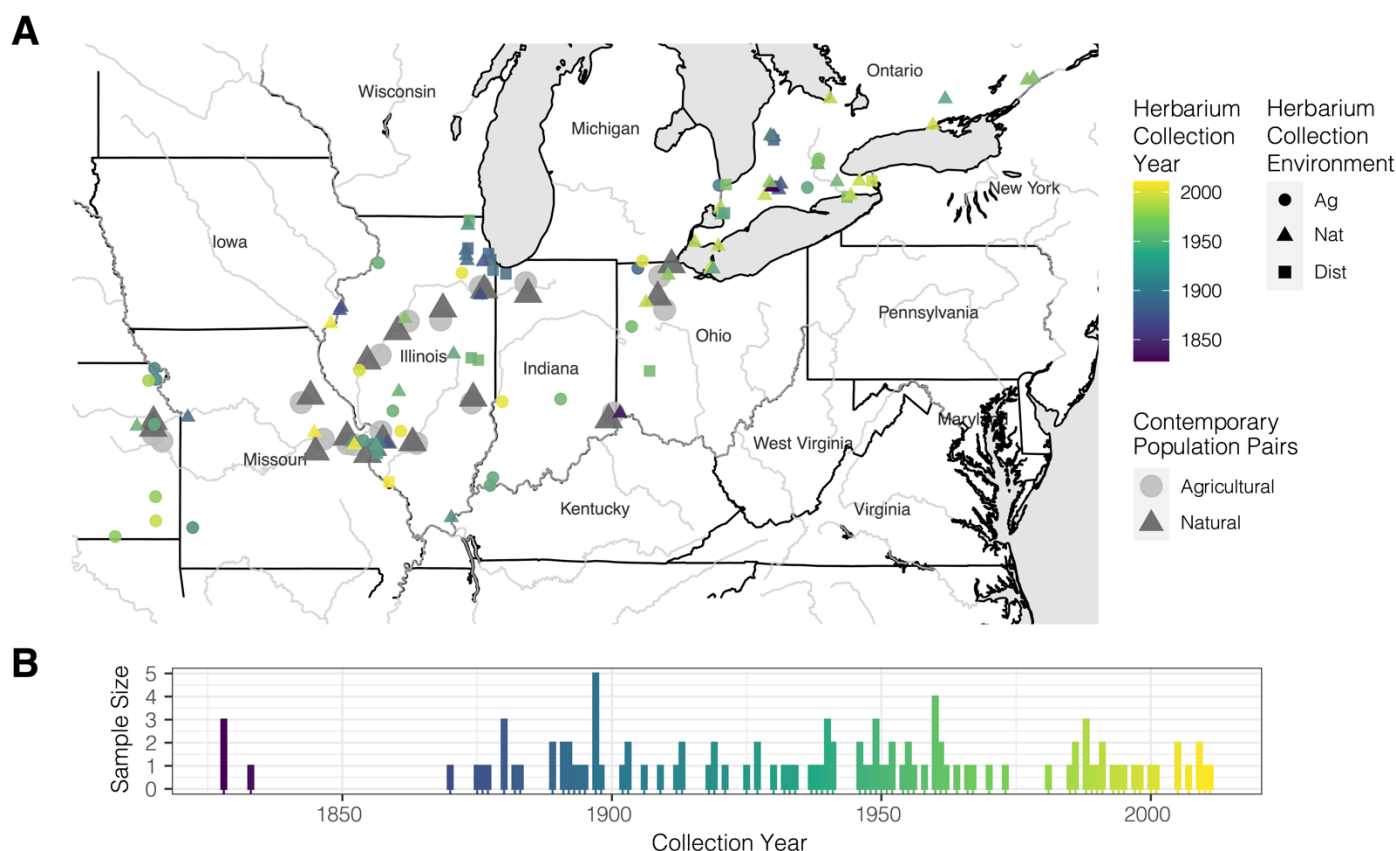


Fig 1. Sequenced waterhemp collections through space and time. A) Map of 17 contemporary paired natural-agricultural populations [$n=187$, collected and sequenced in Kreiner et al., 2021 (24)], along with 108 novel sequenced herbarium specimens dating back to 1828 collected across three environment types (Ag=Agricultural, Nat=Natural, Dist=Disturbed). **B)** Distribution of sequenced herbarium samples through time.

The genome-wide signatures of agricultural adaptation

To find alleles favored under current farming practices, we looked for those alleles that were consistently overrepresented in extant populations collected in agricultural habitats compared to neighboring riparian (“natural”) habitats (24) using Cochran–Mantel–Haenszel (CMH) tests (**Fig 2A**). Alleles associated with agricultural environments (the 0.1% of SNPs with lowest CMH p-values; $n=7264$) are significantly enriched for 29 GO-biological process terms related to growth and development, reproduction, cellular metabolic processes, and responses to abiotic, endogenous and external stimuli, including response to chemicals (**Table S1**). The importance of chemical inputs in shaping weed agricultural adaptation is clear in that the most significant agriculturally associated SNP (raw p-value = 8.551×10^{-11} , [FDR corrected] q-value = 0.00062) falls just 80 kb outside the gene protoporphyrinogen oxidase (*PPO*)—the target of PPO-inhibiting herbicides (**Fig 2B**). PPO herbicides were widely used in the 1990s, but have seen a recent resurgence to control and slow the spread of glyphosate resistant weeds (25, 26). Other

genes with the strongest agricultural associations include *ACO1*, which has been shown to confer oxidative stress tolerance (27); *HB13*, involved in pollen viability (28) as well as drought and salt tolerance (29); *PME3*, involved in growth via germination timing (30); *CAM1*, a regulator of senescence in response to stress (31, 32); and both *CRY2* and *CPD*, two key regulators of photomorphogenesis and flowering via brassinosteroid signaling (33–36) (**Table S2**). Natural-vs-agricultural F_{ST} (allele frequency differentiation) is highly correlated with the CMH test statistic (Pearson's $r = 0.987$), with 78% [98%] of CMH focal SNPs overlapping with the top 0.01% [0.1%] of F_{ST} hits (**Fig S1**). Despite negligible genome-wide differentiation ($F_{ST} = 0.0008$; with even lower mean F_{ST} between paired sites = -0.0029; **Fig 2C**) and thus widespread gene flow among environments, our results suggest that strong antagonistic selection acts to maintain spatial differentiation for some alleles—403 SNPs with a CMH q-value < 0.10.

To further investigate the extent to which herbicides shape adaptation to agriculture, we assayed patterns of environmental differentiation at known resistance variants. Eight such alleles were present in contemporary samples, only six of which were common (**Table S3**): a deletion of codon 210 within *PPO* (37), a copy number amplification and a non-synonymous mutation within 5-enolpyruvylshikimate-3-phosphate synthase (*EPSPS*) conferring resistance to glyphosate herbicides (38), and 3 separate non-synonymous mutations within acetolactate synthase (*ALS*) conferring resistance to ALS-inhibiting herbicides (18). While these resistance alleles were at intermediate frequency in agricultural populations, ranging from 0.08 to 0.35, they tended to be rarer but still frequent in natural populations, ranging from 0.04 to 0.22. Three out of six common resistance alleles showed significant allele frequency differences among environments (*EPSPS*amp: $F = 8.74$, $p = 0.006$; *PPO*210: $F = 40.98$; $p = 1.25e-09$; *ALS*574: $F = 6.28$; $p = 0.013$), two of which showed some of the strongest signals of differentiation genome-wide. Natural-vs-agricultural F_{ST} at the *PPO*210 deletion, 0.21, is higher than anywhere else in the genome and is even stronger when calculated within population pairs ($F_{ST} = 0.27$) (**Fig 2C**). Similarly, the *EPSPS* amplification is ranked 20th among genome-wide biallelic F_{ST} values, 0.14 (within-pair $F_{ST} = 0.22$), in support of herbicides as a foremost driver of agricultural adaptation (**Fig 2D**).

To infer the importance of selective trade-offs in adaptation across natural and agricultural environments, we implemented a Wright-Fisher allele-frequency-based migration-selection balance model for these three differentiated resistance alleles, as well as the top 30 independent CMH outliers. Assuming these alleles are at a steady-state between migration and selection, we inferred that the costs of resistance per migrant that has arrived into natural environments are consistently higher than the benefits of resistance per migrant that has arrived into agricultural environments (per-migrant cost: benefit ratio ranges from 1.38 for *EPSPS*amp and 1.44 for *ALS*574, to 5.02 for the *PPO*210 deletion; **Fig 2D**, **Table S3**). Thus, the spread of these three common herbicide resistance alleles appears to be constrained either by more consistent selection against resistance in herbicide-free, natural environments, or by particularly high rates of

migration of susceptible alleles from natural into agricultural environments. In comparison, for the top 30 independent CMH outliers, the costs per migrant that has arrived in natural environments were about equally likely to be stronger or weaker (12/28, 42%) than the benefits per migrant in agricultural environments (**Fig S2**). Although further work is necessary to understand the contributions of temporal and spatial heterogeneity in both migration and selection for and against resistance across the landscape, these first results suggest that costs of resistance in the absence of herbicides may play an important role.

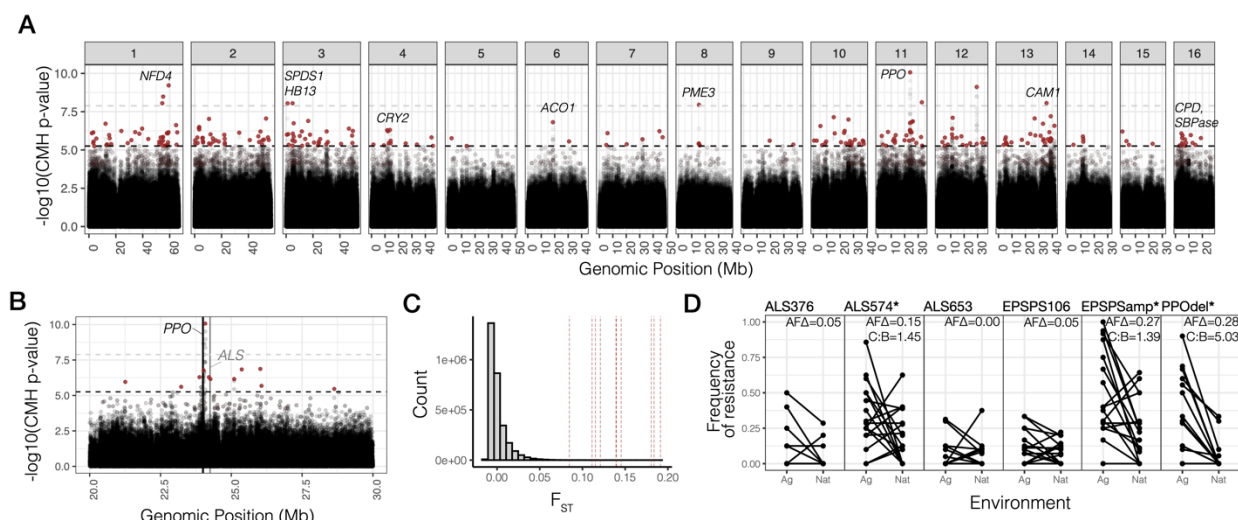


Fig 2. Signals of contemporary agricultural adaptation, gene flow, and antagonistic selection across the genome in *A. tuberculatus*. **A)** Results from Cochran–Mantel–Haenszel (CMH) tests for SNPs with consistent differentiation among environments across contemporary natural-agricultural population pairs. A 10% FDR threshold is indicated by the lower dashed horizontal black line, while the Bonferroni corrected p-value < 0.1 cutoff is shown by the upper dashed horizontal gray line. Red points indicate focal adaptive SNPs after aggregating linked variation ($r^2 > 0.25$ within 1 Mb). Candidate agriculturally adaptive genes for peaks that are significant at a 10% FDR threshold shown. **B)** CMH results from the scaffold containing the most significant CMH p-value, corresponding to variants linked to the PPO210 deletion conferring herbicide resistance and to the nearby herbicide-targeted gene *ALS*. **C)** Distribution of F_{ST} values between all agricultural and natural samples for ~3 million genome-wide SNPs (minor allele frequency > 0.05). Vertical lines indicate F_{ST} values for the 10 candidate genes named in **A**. **D)** Population-level frequencies of six common herbicide resistance alleles across geographically paired agricultural and natural habitats sampled in 2018 (pairs connected by horizontal lines). The first four columns are nonsynonymous variants in *ALS* and *EPSPS*, followed by EPSPSamp (a 10 Mb-scale amplification that includes *EPSPS*), and lastly, an in-frame single-codon deletion in *PPO*. Estimates of per-migrant natural cost: agricultural benefit ratio (C:B) is shown in the top right corner for the three resistance alleles with a significant (*) allele frequencies differences (AFA) across environment types.

Agriculturally-adaptive alleles change rapidly with intensified regimes

With a genome-wide set of agriculture-associated alleles (251 loci after aggregating linked SNPs), we searched for signatures of temporal evolution using newly collected whole genome sequence data from a set of historical herbarium samples ($n=108$) dating back to 1828. These samples provide snapshots of the genetic changes that have occurred over this time period and across environment types, with collections from natural and weedy (agricultural and disturbed) habitats (**Fig 1**). Of the 165 loci for which we had sufficient information in the historical SNP set (sequenced to 10x coverage on average), 151 were segregating with the same reference/alternate allele combination (i.e. 11 were dropped due to multi-allelism), and only three were invariant. To model allele frequency change through time at these alleles, we implemented logistic regressions of genotypes (within individual allele frequencies) at each locus on collection year, where $2 \times \text{slope}$ of the logit-transform is equivalent to the strength of selection (s) in a diploid model of selection (where s is the fitness difference between homozygotes, assuming additivity; see *Methods* for model and simulations (39)).

Consistent with the rapid change in land use and farming practices in the recent past, the frequency of these 154 contemporary agricultural alleles has increased substantially over the last two centuries. Whereas in natural environments agriculturally-adaptive alleles have increased by 6% on average since 1870, the earliest time point at which we have collections across environment types, these same alleles have increased by 22% in disturbed and agricultural environments (**Fig 3A**). This observed change greatly exceeds the expected change over this time period, based on genome-wide patterns that reflect drift, migration, selection, and demographic change (null 95% interquantile range for allele frequency change in agricultural and disturbed sites = [3.3, 7.9%]; for change in natural sites = [-2.7, 2.0.%]). We generated these null expectations by randomly sampling a set of 154 loci with the same distribution of contemporary allele frequencies (**Fig S4**) and calculating their frequency change through time across herbarium samples, separately in each environment, 1000 times (see *Methods* (39)). That the observed change in natural environments is also more extreme than what is expected is consistent with ongoing migration of agriculturally-selected alleles and subsequent costs in natural environments.

The considerable increase in frequency of these alleles across environments corresponds to remarkably strong selection even when estimated over century-long time periods. The 154 agriculture-associated alleles collectively exhibit a selective strength of $\tilde{s} = 0.022$ since the 1870s in agricultural and disturbed habitats but exhibit much weaker selection, $\tilde{s} = 0.0056$, in natural habitats (agricultural and disturbed null interquantile range = [0.0026, 0.0068]; natural null interquantile range = [-0.0018, 0.0018]). An open question in evolutionary biology is what distribution of selection coefficients underlie adaptation (40). We estimate that selection on agricultural-associated loci varies between -0.196 and 0.150 in natural habitats, and -0.090 and 0.372 in agricultural and disturbed habitats,

reflective of left and right skewed distributions respectively (**Fig 3B, Fig S5**). The top 15 agriculture-associated alleles that we infer have experienced the strongest, significant selection over the last ~150 years include SNPs that map near *PPO*, *ACO1*, *CCB2*, *WRKY13*, *BPL3*, and *ATPD* (**Table S4**). We find that both the total frequency change of agriculture-associated alleles and the estimated strength of selection in agricultural and disturbed environments are positively correlated with the extent of contemporary linkage disequilibrium around these loci (the number of SNPs with $r^2 > 0.25$ within 1Mb) (frequency change: $F = 5.16$, $p = 0.024$, $r = 0.12$; strength of selection: $F = 3.99$, $p = 0.048$, $r = 0.058$; **Fig S6**), consistent with theoretical expectations for the genomic signatures of recent positive selection (41, 42).

We next asked how well the trajectory of modern agricultural alleles mimic the rise of industrialized agricultural regimes across the last century. When we split out samples into those that predate versus those that come after the intensification of agriculture during the Green Revolution, we find that the increase in frequency of agricultural alleles was negligible in agricultural and disturbed environments before the 1960s (predicted 1870-1960 change = 0.005). In contrast, change subsequent to 1960 nearly completely accounts for the observed rise in frequency of modern agricultural alleles (predicted 1960-2018 change = 0.219, versus total 1870-2018 change = 0.221) (**Fig 3C**). Corresponding estimates of selection by logistic regression using only data from before 1960 shows no evidence of selection on these loci in disturbed and agricultural habitats ($\tilde{s} = 0.0008$, null interquantile range = [-0.0044, 0.0020]) or in natural habitats ($\tilde{s} = 0.0006$, null interquantile range = [-0.004, 0.004]). However, samples collected after 1960 reflect a dramatic shift in selection—a collective $\tilde{s} = 0.054$ in disturbed and agricultural environments and a collective $\tilde{s} = 0.028$ in natural environments (agricultural/disturbed null interquantile range = [0.0064, 0.0020]; natural null interquantile range = [-0.0056, 0.0054]) (**Fig 3C; Fig S8**). Together, these results suggest that while most contemporary agricultural alleles were present in historical populations, these alleles only became associated with agricultural and human-managed sites over the last century, on timescales and rates consistent with the rapid uptake and intensification of agrochemicals, controlled irrigation, and mechanization in agriculture.

The historical trajectory of known herbicide resistance alleles epitomizes extreme selection over the last 50 years (**Fig 3D**). Five out of seven known biallelic herbicide resistance alleles present in our contemporary, paired-environment collections are absent from our historical samples, consistent with the suggested importance of resistance adaptation from *de novo* mutation (12, 43) and a particularly recent increase in their frequency. Only three out of 108 historical samples show variation for herbicide resistance, two samples homozygous for resistance at ALS574 and one heterozygous for resistance at ALS122—all of which were sampled after the onset of herbicide applications in the 1960s (**Fig 3D**). Resolving the very low historical and much higher contemporary frequencies of resistance, we estimate that since the approximate onset of herbicide use in 1960, these seven resistance alleles have collectively experienced a

selective strength of $\tilde{s} = 0.198$ ($Z = 2.11$, $p = 0.035$) per year. Independently estimated selective strengths are significant for five of the seven resistance alleles, strongest for PPO210 ($s > 0.194$), EPSPS106 ($s > 0.106$), and for ALS574 ($s > 0.088$) (Fig 3D; Table S3). As expected, selection has been particularly strong on these alleles collectively in agricultural environments ($\tilde{s} = 0.200$, $Z = 2.121$, $p = 0.034$), with no significant evidence of selection on resistance alleles in any other distinct habitat type.

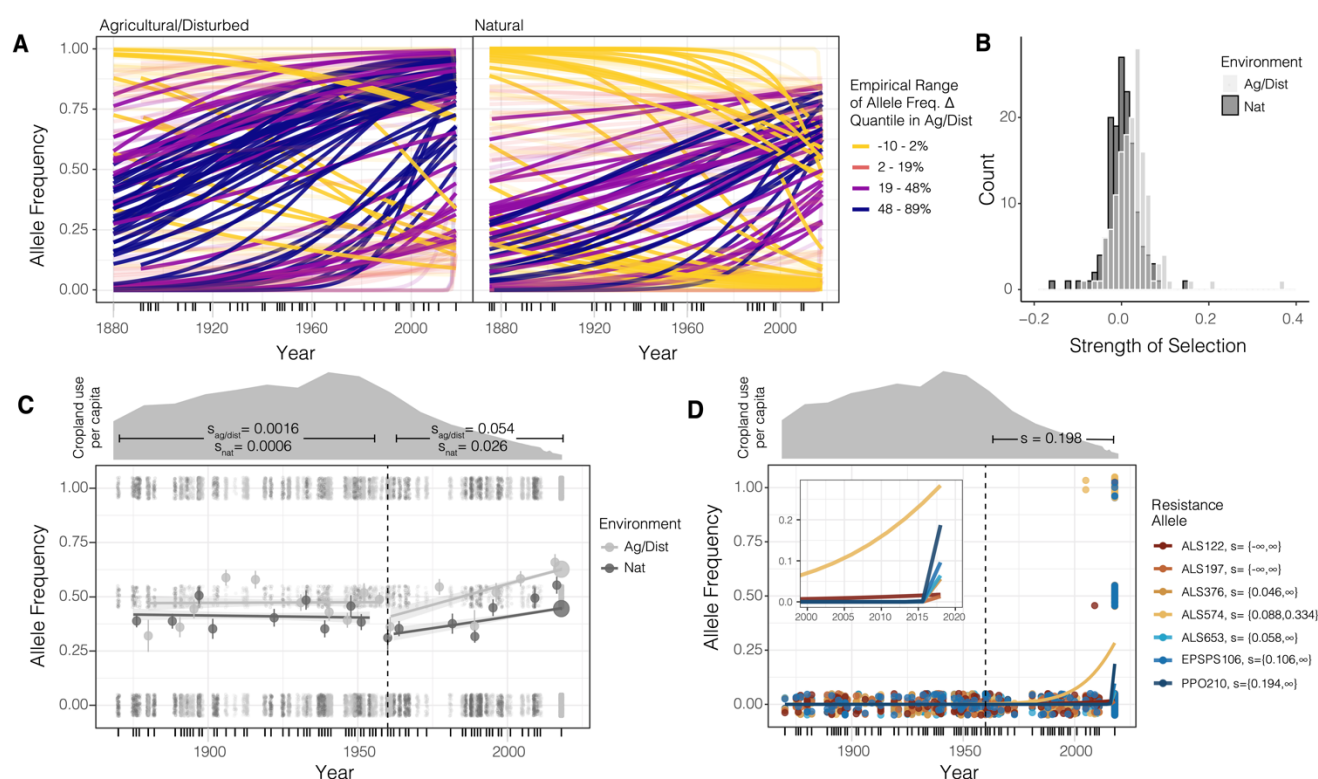


Fig 3. Genomic signatures of agricultural adaptation through time. **A)** Agricultural allele frequency trajectories for each 154 focal SNPs, in agricultural and disturbed habitats (left), and natural habitats (right). Trajectories colored by the empirical quantile of frequency change in agricultural and disturbed habitats. Transparent lines indicate those with non-significant evidence of selection at $\alpha=0.05$ after FDR=10% correction. **B)** The distribution of selective strengths on agricultural alleles in natural (dark gray) and agricultural/disturbed (light gray) habitats between 1870 and 2018. **C)** Environment-specific agricultural allele frequency trajectories, before and after the start of agricultural intensification in 1960 (vertical dashed line). Large circles represent moving averages (over both loci and individuals) of allele frequencies, whereas dots represent raw genotype data for each locus and sample from which the allele frequency trajectory is estimated. Cropland use per capita in North America data from (1), rescaled by use in 1600, to reflect intensity of agricultural practices. **D)** The trajectory of alleles at known herbicide resistance loci through time, fit by logistic regression for each of the biallelic resistance alleles present in our contemporary data (excluding EPSPSamp with its complex allelic structure). Dots represent genotypes for each historical and contemporary sample at each herbicide resistance locus. 95% credible interval of the maximum likelihood estimate of selection between 1960-2018 provided in the legend for each resistance allele.

Concurrent temporal shifts in ancestry underlie agricultural adaptation

Finally, we explored whether historical demographic change over the last two centuries has played a role in agricultural adaptation. Early taxonomy described two different *A. tuberculatus* varieties as separate species, with few distinguishing characteristics (seed dehiscence and tepal length (15)). Sauer's 1955 revision of the genus, which used herbarium specimens to gauge the distribution and migration of congeners over the last two centuries (44), led him to describe an expansion of the southwestern var. *rudis* type (at the time, *A. tamariscinus* (Sauer)) northeastward into the territory of var. *tuberculatus* (*A. tuberculatus* (Sauer)), sometime between 1856-1905 and 1906-1955. Our sequencing of over 100 herbarium samples dating back to 1828, combined with 349 contemporary sequences (24, 45), allowed us to directly observe the change in the distribution of these two ancestral types, adding further temporal resolution to Sauer's morphological observations of the species' range shifts, and to assess the role of agriculturally-adaptive standing genetic variation across varieties.

Range-wide, we see clear shifts in the distribution of var. *rudis* ancestry based on fastSTRUCTURE (46) inference at K=2 (**Fig S9**) across three-time spans, 1830-1920, 1920-1980, and 1980-2018 (timespan: $F = 5.47$, $p = 0.0045$), and particularly so in the East (timespan x longitude: $F = 5.49$, $p = 0.0045$), consistent with a recent expansion of var. *rudis* ancestry (**Fig 4A**). Furthermore, we see strong state and province-specific shifts in ancestry through time in our historical sequences (time span by state interaction: $F = 4.22$, $p = 7 \times 10^{-5}$), highlighting not only the shift of var. *rudis* eastwards (with increases through time in Ontario, Ohio, Illinois, and Missouri) but also the very recent introduction of var. *tuberculatus* ancestry into the most western part of the range in Kansas (**Fig 4B**). *A. tuberculatus* demography thus appears to have been drastically influenced by human-mediated landscape change over the last two centuries, consistent with the massive recent expansion of effective population size we have previously inferred from contemporary samples over this same timeframe (43). That this shift has been most notable over the last 40 years is further consistent with the timescale of agricultural intensification, shifts towards conservation tillage, and rampant herbicide resistance evolution within the species (18, 43, 47, 48), suggesting selection on resistance may facilitate the colonization of var. *rudis* ancestry outside its historical range. Along these lines, we find this contemporary expansion has facilitated the sorting of var. *rudis* ancestry across environments (a longitude by time span by environment interaction: $F = 5.13$, $p = 4 \times 10^{-5}$; **Fig 4C**), with increasing overrepresentation of var. *rudis* ancestry in agricultural and disturbed environments in the eastern portion of the range through time, as previously suggested (24).

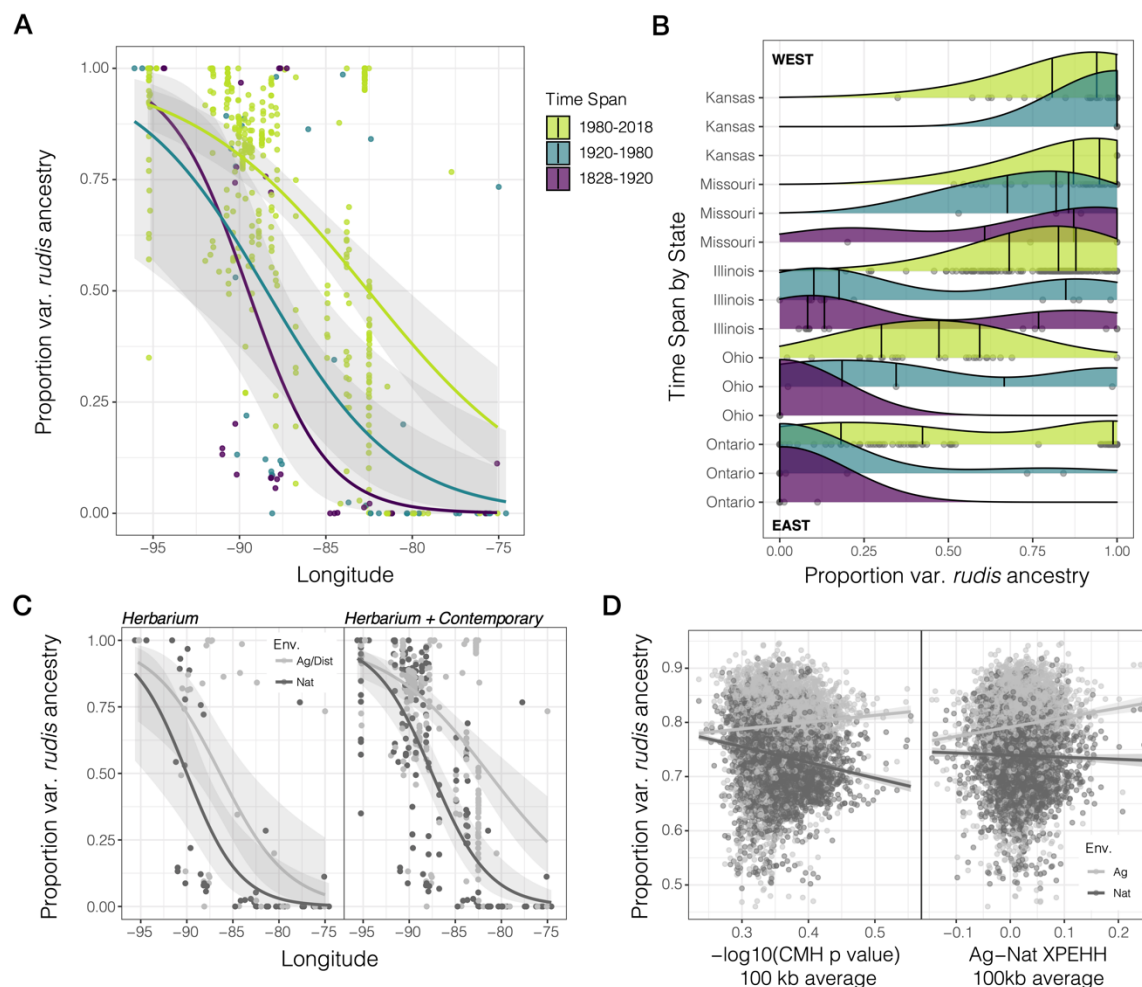


Fig 4. Temporal shifts in the distribution of var. *rudis* ancestry have facilitated polygenic agricultural adaptation. **A)** Longitudinal clines in individual-level var. *rudis* ancestry over three timespans, illustrating the expansion of var. *rudis* ancestry eastwards over the last two centuries. **B)** The distribution of individual-level var. *rudis* ancestry by state and through time, illustrating state-specific changes in ancestry. Vertical lines represent first, second, and third quantiles of ancestry within each timespan and state. Timespans indicated in (A). No individuals were collected from Kansas between 1828-1920. **C)** Increasing sorting of individual-level var. *rudis* ancestry into agricultural environments on contemporary timescales. **D)** Environment-specific metrics of selection (CMH p-value and cross-population extended haplotype homozygosity (XPEHH)) across the genome in 100 kb windows positively correlate with var. *rudis* ancestry in agricultural, but not natural habitats (XPEHH by Environment: $F=9.34$, $p=0.002$; CMH by Environment: $F=99.70$, $p < 10^{-16}$).

To investigate whether agricultural adaptation has drawn disproportionately from var. *rudis* ancestry, we reconstructed fine-scale ancestry across the genome. Based on analyses in 100 kb windows, we find a least-squares mean of 5.5% (95% CI = [5.0, 5.9%]) more var. *rudis* ancestry genome-wide in agricultural environments compared to the adjacent natural habitat (**Fig S10**). The environment-specific proportion of var. *rudis*

ancestry is not only positively correlated with recombination rate ($F = 16.67$, $p = 4.5 \times 10^{-5}$, $r = 0.056$) and gene density ($F = 5.85$, $p = 0.016$, $r = 0.499$) but also with SNP and haplotype-based evidence of environment-specific selection. Agricultural, but not natural populations, have an excess of cross-population haplotype homozygosity (agricultural vs. natural XPEHH) and within-pair environmental differentiation (CMH p-value) in genomic regions of high var. *rudis* ancestry (XPEHH by Environment: $F=9.34$, $p=0.002$; CMH by Environment: $F=99.70$, $p < 10^{-16}$; **Fig 4D**), implying that ancestry composition genome-wide in large part determines the extent of polygenic agricultural adaptation. These findings suggest that the expansion of var. *rudis* ancestry across the range, particularly in the last 40 years, has facilitated waterhemp's success in agricultural habitats through providing access to preadapted, standing genetic variation.

Discussion

Agricultural adaptation in *A. tuberculatus*, a native plant in North America, has occurred over extremely rapid timescales, facilitated by range shifts in response to the agriculturalization of its native habitat. The human-mediated expansion of the southwestern lineage of the species northeastwards since the latter half of the 20th century has introduced new genetic variation across the range and across the genome, on which selection in agricultural settings could act. Negligible genetic differentiation across habitats in this species refutes the idea of agriculture existing as separate to natural ecosystems (49). Despite substantial gene flow and concurrent with the intensification of agriculture, the prevalence of agricultural alleles has increased rapidly over just the last 60 years, in agricultural environments by nearly 6% per year, and even in natural sites by more than 2% per year. The empirical estimates of selection coefficients for herbicide resistance provided here—20% per year range-wide over a 60-year period—emphasizes the rapid and lasting impact of agricultural herbicides across heterogeneous environments. While modern, industrial agriculture imposes strengths of selection rarely observed in the wild, this species has in turn escalated the weed management-evolution arms race through a multitude of interdependent mechanisms: range expansion, polygenic adaptation from standing genetic variation, and large effect herbicide resistance mutations.

Together, these results highlight that anthropogenic change not only leads to the formation of new habitats but also provides an opportunity for range expansion that may facilitate and feedback with local adaptation, reshaping genetic variation for fitness within native and potentially weedy species.

References and Notes

1. K. Klein Goldewijk, A. Beusen, J. Doelman, E. Stehfest, Anthropogenic land use estimates for the Holocene – HYDE 3.2. *Earth Syst. Sci. Data*. **9**, 927–953 (2017).
2. T. G. Benton, J. A. Vickery, J. D. Wilson, Farmland biodiversity: is habitat heterogeneity the key? *Trends in Ecology & Evolution*. **18** (2003), pp. 182–188.
3. E. Malaj, L. Freistadt, C. A. Morrissey, Spatio-temporal patterns of crops and agrochemicals in Canada over 35 years. *Front. Environ. Sci.* **8** (2020), doi:10.3389/fenvs.2020.556452.
4. J. Fernandez-Cornejo, R. F. Nehring, C. Osteen, S. Wechsler, A. Martin, A. Vialou, Pesticide use in U.s. agriculture: 21 selected crops, 1960-2008. *SSRN Electron. J.* (2014), doi:10.2139/ssrn.2502986.
5. N. E. Borlaug, Contributions of conventional plant breeding to food production. *Science*. **219**, 689–693 (1983).
6. H. J. Beckie, K. N. Harker, L. M. Hall, S. I. Warwick, A. Légère, P. H. Sikkema, G. W. Clayton, A. G. Thomas, J. Y. Leeson, G. Séguin-Swartz, M.-J. Simard, A decade of herbicide-resistant crops in Canada. *Can. J. Plant Sci.* **86**, 1243–1264 (2006).
7. C. Mann, Reseeding the Green Revolution. *Science* (1997), doi:10.1126/science.277.5329.1038.
8. P. L. Pingali, Green revolution: impacts, limits, and the path ahead. *Proc. Natl. Acad. Sci. U. S. A.* **109**, 12302–12308 (2012).
9. P. Pellegrini, R. J. Fernández, Crop intensification, land use, and on-farm energy-use efficiency during the worldwide spread of the green revolution. *Proc. Natl. Acad. Sci. U. S. A.* **115**, 2335–2340 (2018).
10. J. Mallet, The evolution of insecticide resistance: Have the insects won? *Trends Ecol. Evol.* **4**, 336–340 (1989).
11. C. Délye, M. Jasieniuk, V. Le Corre, Deciphering the evolution of herbicide resistance in weeds. *Trends Genet.* **29**, 649–658 (2013).
12. N. J. Hawkins, C. Bass, A. Dixon, P. Neve, The evolutionary origins of pesticide resistance. *Biol. Rev. Camb. Philos. Soc.* (2018), doi:10.1111/brv.12440.
13. F. Gould, Z. S. Brown, J. Kuzma, Wicked evolution: Can we address the sociobiological dilemma of pesticide resistance? *Science*. **360**, 728–732 (2018).
14. F. Zabel, R. Delzeit, J. M. Schneider, R. Seppelt, W. Mauser, T. Václavík, Global impacts of future cropland expansion and intensification on agricultural markets and biodiversity. *Nat. Commun.* **10**, 2844 (2019).

- 476 15. J. Sauer, REVISION OF THE DIOECIOUS AMARANTHS. *Madroño*. **13**, 5–46 (1955).
- 477 16. K. E. Waselkov, K. M. Olsen, Population genetics and origin of the native North American
478 agricultural weed waterhemp (*Amaranthus tuberculatus*; *Amaranthaceae*). *Am. J. Bot.* **101**,
479 1726–1736 (2014).
- 480 17. M. Costea, S. E. Weaver, F. J. Tardif, The Biology of Invasive Alien Plants in Canada. 3.
481 *Amaranthus tuberculatus* (Moq.) Sauer var. *rudis* (Sauer) Costea & Tardif. *Can. J. Plant*
482 *Sci.* **85**, 507–522 (2005).
- 483 18. P. J. Tranel, Herbicide resistance in *Amaranthus tuberculatus*†. *Pest Manag. Sci.* **77**, 43–54
484 (2021).
- 485 19. J. Hermisson, P. S. Pennings, Soft sweeps: molecular population genetics of adaptation
486 from standing genetic variation. *Genetics*. **169**, 2335–2352 (2005).
- 487 20. R. D. H. Barrett, D. Schluter, Adaptation from standing genetic variation. *Trends Ecol.*
488 *Evol.* **23**, 38–44 (2008/1).
- 489 21. M. Alleaume-Benharira, I. R. Pen, O. Ronce, Geographical patterns of adaptation within a
490 species’ range: interactions between drift and gene flow. *J. Evol. Biol.* **19**, 203–215 (2006).
- 491 22. R. I. Colautti, S. C. H. Barrett, Rapid adaptation to climate facilitates range expansion of an
492 invasive plant. *Science*. **342**, 364–366 (2013).
- 493 23. M. Szűcs, M. L. Vahsen, B. A. Melbourne, C. Hoover, C. Weiss-Lehman, R. A. Hufbauer,
494 Rapid adaptive evolution in novel environments acts as an architect of population range
495 expansion. *Proc. Natl. Acad. Sci. U. S. A.* **114**, 13501–13506 (2017).
- 496 24. J. M. Kreiner, A. Caballero, S. I. Wright, J. R. Stinchcombe, Selective ancestral sorting and
497 de novo evolution in the agricultural invasion of *Amaranthus tuberculatus*. *Evolution*
498 (2021), doi:10.1111/evo.14404.
- 499 25. F. E. Dayan, S. O. Duke, in *Hayes’ Handbook of Pesticide Toxicology*, R. Krieger, Ed.
500 (Academic Press, New York, 2010), pp. 1733–1751.
- 501 26. J. G. Moraes, T. R. Butts, V. M. Anunciato, J. D. Luck, W. C. Hoffmann, U. R. Antuniassi,
502 G. R. Kruger, Nozzle selection and adjuvant impact on the efficacy of glyphosate and PPO-
503 inhibiting herbicide tank-mixtures. *Agronomy (Basel)*. **11**, 754 (2021).
- 504 27. W. Moeder, O. Del Pozo, D. A. Navarre, G. B. Martin, D. F. Klessig, Aconitase plays a role
505 in regulating resistance to oxidative stress and cell death in *Arabidopsis* and *Nicotiana*
506 *benthamiana*. *Plant Mol. Biol.* **63**, 273–287 (2007).
- 507 28. P. A. Ribone, M. Capella, R. L. Chan, Functional characterization of the homeodomain
508 leucine zipper I transcription factor AtHB13 reveals a crucial role in *Arabidopsis*
509 development. *J. Exp. Bot.* **66**, 5929–5943 (2015).

29. J. V. Cabello, R. L. Chan, The homologous homeodomain-leucine zipper transcription factors HaHB1 and AtHB13 confer tolerance to drought and salinity stresses via the induction of proteins that stabilize membranes. *Plant Biotechnol. J.* **10**, 815–825 (2012).
30. S. Guénin, J. Hardouin, F. Paynel, K. Müller, G. Mongelard, A. Driouich, P. Lerouge, A. R. Kermode, A. Lehner, J.-C. Mollet, J. Pelloux, L. Gutierrez, A. Mareck, AtPME3, a ubiquitous cell wall pectin methylesterase of *Arabidopsis thaliana*, alters the metabolism of cruciferin seed storage proteins during post-germinative growth of seedlings. *J. Exp. Bot.* **68**, 1083–1095 (2017).
31. S. Zhou, L. Jia, H. Chu, D. Wu, X. Peng, X. Liu, J. Zhang, J. Zhao, K. Chen, L. Zhao, *Arabidopsis* CaM1 and CaM4 Promote Nitric Oxide Production and Salt Resistance by Inhibiting S-Nitrosogluthathione Reductase via Direct Binding. *PLoS Genet.* **12**, e1006255 (2016).
32. C. Dai, Y. Lee, I. C. Lee, H. G. Nam, J. M. Kwak, Calmodulin 1 Regulates Senescence and ABA Response in *Arabidopsis*. *Front. Plant Sci.* **9**, 803 (2018).
33. H. Guo, H. Yang, T. C. Mockler, C. Lin, Regulation of flowering time by *Arabidopsis* photoreceptors. *Science*. **279**, 1360–1363 (1998).
34. T. Mockler, H. Yang, X. Yu, D. Parikh, Y.-C. Cheng, S. Dolan, C. Lin, Regulation of photoperiodic flowering by *Arabidopsis* photoreceptors. *Proc. Natl. Acad. Sci. U. S. A.* **100**, 2140–2145 (2003).
35. W. Wang, X. Lu, L. Li, H. Lian, Z. Mao, P. Xu, T. Guo, F. Xu, S. Du, X. Cao, S. Wang, H. Shen, H.-Q. Yang, Photoexcited CRYPTOCHROME1 Interacts with Dephosphorylated BES1 to Regulate Brassinosteroid Signaling and Photomorphogenesis in *Arabidopsis*. *Plant Cell*. **30**, 1989–2005 (2018).
36. J. Li, Y. Li, S. Chen, L. An, Involvement of brassinosteroid signals in the floral-induction network of *Arabidopsis*. *J. Exp. Bot.* **61**, 4221–4230 (2010).
37. F. E. Dayan, P. R. Daga, S. O. Duke, R. M. Lee, P. J. Tranel, R. J. Doerksen, Biochemical and structural consequences of a glycine deletion in the α -8 helix of protoporphyrinogen oxidase. *Biochimica et Biophysica Acta (BBA) - Proteins and Proteomics*. **1804**, 1548–1556 (2010).
38. H. M. Cockerton, S. S. Kaundun, L. Nguyen, S. J. Hutchings, R. P. Dale, A. Howell, P. Neve, Fitness cost associated with enhanced EPSPS gene copy number and glyphosate resistance in an *Amaranthus tuberculatus* population. *Cold Spring Harbor Laboratory* (2021), p. 2021.01.09.426028, , doi:10.1101/2021.01.09.426028.
39. Kreiner, J.M. Latorre, S.M., Burbano, H.A., Stinchcombe, J.R., Otto, S.P., Weigel, D., Wright, S., Materials and Methods for “200 years of agricultural adaptation and range expansion in a native weed.” *Science*.
40. N. H. Barton, The “New Synthesis.” *Proceedings of the National Academy of Sciences*. **119**,

547 e2122147119 (2022).

548 41. M. Przeworski, The signature of positive selection at randomly chosen loci. *Genetics*. **160**,
549 1179–1189 (2002).

550 42. Y. Kim, R. Nielsen, Linkage disequilibrium as a signature of selective sweeps. *Genetics*.
551 **167**, 1513–1524 (2004).

552 43. J. M. Kreiner, G. Sandler, A. J. Stern, P. J. Tranel, D. Weigel, J. Stinchcombe, S. I. Wright,
553 Repeated origins, widespread gene flow, and allelic interactions of target-site herbicide
554 resistance mutations. *Elife*. **11**, e70242 (2022).

555 44. J. Sauer, Recent Migration and Evolution of the Dioecious Amaranths. *Evolution*. **11**, 11–31
556 (1957).

557 45. J. M. Kreiner, D. A. Giacomini, F. Bemm, B. Waithaka, J. Regalado, C. Lanz, J.
558 Hildebrandt, P. H. Sikkema, P. J. Tranel, D. Weigel, J. R. Stinchcombe, S. I. Wright,
559 Multiple modes of convergent adaptation in the spread of glyphosate-resistant *Amaranthus*
560 *tuberculatus*. *Proc. Natl. Acad. Sci. U. S. A.* **116**, 21076–21084 (2019).

561 46. A. Raj, M. Stephens, J. K. Pritchard, fastSTRUCTURE: variational inference of population
562 structure in large SNP data sets. *Genetics*. **197**, 573–589 (2014).

563 47. M. J. Foes, L. Liu, P. J. Tranel, L. M. Wax, E. W. Stoller, A biotype of common waterhemp
564 (*Amaranthus rudis*) resistant to triazine and ALS herbicides. *Weed Sci.* **46**, 514–520 (1998).

565 48. P. J. Tranel, C. W. Riggins, M. S. Bell, A. G. Hager, Herbicide resistances in *Amaranthus*
566 *tuberculatus*: a call for new options. *J. Agric. Food Chem.* **59**, 5808–5812 (2011).

567 49. Q. C. B. Cronk, J. L. Fuller, *Plant invaders: The threat to natural ecosystems* (Routledge,
568 2014).

569 50. S. M. Latorre, P. L. M. Lang, H. A. Burbano, R. M. Gutaker, Isolation, Library Preparation,
570 and Bioinformatic Analysis of Historical and Ancient Plant DNA. *Curr Protoc Plant Biol.*
571 **5**, e20121 (2020).

572 51. S. Chen, Y. Zhou, Y. Chen, J. Gu, fastp: an ultra-fast all-in-one FASTQ preprocessor.
573 *Bioinformatics*. **34** (2018), pp. i884–i890.

574 52. H. Li, R. Durbin, Fast and accurate short read alignment with Burrows-Wheeler transform.
575 *Bioinformatics*. **25**, 1754–1760 (2009).

576 53. A. Peltzer, G. Jäger, A. Herbig, A. Seitz, C. Knip, J. Krause, K. Nieselt, EAGER: efficient
577 ancient genome reconstruction. *Genome Biol.* **17**, 60 (2016).

578 54. H. Jónsson, A. Ginolhac, M. Schubert, P. L. F. Johnson, L. Orlando, mapDamage2.0: fast
579 approximate Bayesian estimates of ancient DNA damage parameters. *Bioinformatics*. **29**,
580 1682–1684 (2013).

55. S. Purcell, B. Neale, K. Todd-Brown, L. Thomas, M. A. R. Ferreira, D. Bender, J. Maller, P. Sklar, P. I. W. de Bakker, M. J. Daly, P. C. Sham, PLINK: a tool set for whole-genome association and population-based linkage analyses. *Am. J. Hum. Genet.* **81**, 559–575 (2007).
56. D. M. Emms, S. Kelly, OrthoFinder: solving fundamental biases in whole genome comparisons dramatically improves orthogroup inference accuracy. *Genome Biol.* **16**, 157 (2015).
57. S. F. Altschul, W. Gish, W. Miller, E. W. Myers, D. J. Lipman, Basic local alignment search tool. *J. Mol. Biol.* **215**, 403–410 (1990).
58. Z. A. Szpiech, R. D. Hernandez, selscan: an efficient multithreaded program to perform EHH-based scans for positive selection. *Mol. Biol. Evol.* **31**, 2824–2827 (2014).
59. O. Delaneau, J.-F. Zagury, J. Marchini, Improved whole-chromosome phasing for disease and population genetic studies. *Nat. Methods.* **10**, 5–6 (2013).
60. F. J. Tardif, I. Rajcan, M. Costea, A mutation in the herbicide target site acetohydroxyacid synthase produces morphological and structural alterations and reduces fitness in *Amaranthus powellii*. *New Phytol.* **169**, 251–264 (2006).
61. M. M. Vila-Aiub, S. S. Goh, T. A. Gaines, H. Han, R. Busi, Q. Yu, S. B. Powles, No fitness cost of glyphosate resistance endowed by massive EPSPS gene amplification in *Amaranthus palmeri*. *Planta.* **239**, 793–801 (2014).
62. C. Wu, A. S. Davis, P. J. Tranel, Limited fitness costs of herbicide-resistance traits in *Amaranthus tuberculatus* facilitate resistance evolution. *Pest Manag. Sci.* **74**, 293–301 (2018).
63. M. M. Vila-Aiub, Fitness of Herbicide-Resistant Weeds: Current Knowledge and Implications for Management. *Plants.* **8** (2019), doi:10.3390/plants8110469.
64. S. Gupta, A. Harkess, A. Soble, M. Van Etten, J. Leebens-Mack, R. S. Baucom, Inter-chromosomal linkage disequilibrium and linked fitness cost loci influence the evolution of nontarget site herbicide resistance in an agricultural weed. *bioRxiv* (2021), p. 2021.04.04.438381, , doi:10.1101/2021.04.04.438381.
65. B. Pasaniuc, S. Sankararaman, G. Kimmel, E. Halperin, Inference of locus-specific ancestry in closely related populations. *Bioinformatics.* **25**, i213–21 (2009).

Acknowledgements: We appreciate the pivotal contribution of numerous herbaria towards this research, especially the help of Eric Knox at the Indiana University Herbarium, Jamie Lynn Minnaert-Grote at the University of Illinois INHS Herbarium; Tedesse Mesfin at the University of Ohio Herbarium, Anton Reznicek at the University of Michigan Herbarium, Jim Solomon at the Missouri Botanical Gardens, Caleb Morse at the McGregor Herbarium at the University of Kansas, Tyler Smith and Song Wang at Agricultural and Agrifood Canada, and Deb Metsger and Tim Dickinson at the Royal Ontario Museum. We thank Mike Whitlock and Tom Booker (University of British Columbia), as well as Aneil Agrawal and Tyler Kent (University of Toronto), and Ailene Macpherson (Simon Fraser University) for input on the work; Christa Lanz and Rebecca Schwab (Max Planck Institute) for coordinating sequencing of herbarium samples; Ella Reiter (University of Leipzig) for scheduling and coordinating logistics for clean room facility work; and Patricia Lang, Sonja Kersten and Heike Budde (Max Planck Institute) for advice on molecular protocols troubleshooting.

Funding: JMK was supported by the Biodiversity Research Institute at the University of British Columbia and a Killam Fellowship. SIW was supported by a NSERC discovery grant and a Canada research chair. JRS was supported by a NSERC discovery grant. SPO was supported by NSERC RGPIN-2022-03726. SML, HAB and DW were supported by the Max Planck Society.

Author Contributions: JMK, JRS, and SIW conceptualized the paired sampling design, JMK, HAB, DW, JRS, and SIW conceptualized the use of herbarium data, JMK performed contemporary collections and curated the herbarium samples, SML and HAB conceptualized and designed the molecular work with herbarium specimens, SML coordinated the clean room facility work, JMK and SML performed DNA extraction and library preparations of herbarium tissue, SML oversaw the sequencing of herbarium specimens. JMK performed analyses with input from SPO, SIW, and JRS. SPO wrote the migration-selection balance and maximum likelihood models. JMK wrote and revised the paper with inputs from all authors.

Competing interests: The authors declare that they have no competing interests.

Data and materials availability: All new sequence has been archived at the SRA (BioProject ID PRJNA878842), while scripts and accompanying metadata have been archived on Github at www.github.com/jkreinz/TemporalAdaptation.

Supplementary Materials

This PDF file includes:

Materials & Methods

Figs. S1 to S13

659 Tables S1 to S5
660 References 55-65
661

Supplementary Materials

Materials & Methods

Herbarium collections

In 2019, we obtained 10 mg tissue collections of herbarium specimens from 7 herbaria across Canada and the United States and one governmental organization: the Royal Ontario Museum Herbarium, the Museum of Biological Diversity at Ohio State University Herbarium, the Indiana University Herbarium, the Michigan State University Herbarium, the Illinois Natural History Survey Herbarium, Missouri Botanical Gardens, The McGregor Herbarium at the University of Kansas, and Agriculture and Agrifood Canada. We selected samples to have an even representation of habitats through time. Samples were classified as natural (n=54), agricultural (n=28), or disturbed (n=20) based on collectors' annotations on each plate: any reference to a cultivated field was treated as an 'agricultural' collection; general environmental descriptions such as dry grassland or riverbank was treated as a 'natural' collection; and reference to disturbed soil, railroad tracks, or manicured or managed land was treated as a 'disturbed' collection. For inference of contemporary allele frequency and ancestry change through time, samples collected from disturbed habitats were grouped together with the agricultural category—in both of which waterhemp exists as a weed (**Table S5**). When geographic coordinates were not provided, we referred to the state, county, section, intersection, and landmark descriptions to infer the geographic coordinate of a given sample. In total, we collected samples from 172 specimens, 108 of which were selected for whole-genome sequencing.

Herbarium DNA extractions & library preparations

The work was performed in the ancient DNA lab at the University of Tübingen. For DNA extraction of the herbarium samples, we followed basic protocol 1 outlined in (50). Briefly, under sterile conditions, ~10 mg of each sample was ground and incubated with N-phenacylthiazolium bromide (PTB)-based mix overnight to lyse DNA. After a shredding step with QIAshredder spin columns, DNA was purified and eluted with DNAeasy Mini spin columns. Sequencing libraries were prepared using the basic protocol 2 outlined in (50), performing blunt-end repair, adapter ligation, a fill-in reaction, indexing, and finally PCR amplification (10 cycles) and a cleaning step. The libraries were sequenced on an Illumina NovaSeq instrument on a single flow cell. The sequencing run produced ~3,442 Gb data, an average of 32 Gb per sample.

Mapping, damage correction, SNP calling and filtering

We removed adapters, polyQ tails, and merged reads from herbarium sequencing reads

using fastp (51). Because of the small fragment size of historical DNA, this resulted in a sizable loss of sequence coverage, from 46X coverage to a mean of 11X coverage. Mapping with bwa mem (52), we found on average, 89% of merged reads mapped to the female, US Midwestern, reference genome from (45), suggesting low rates of contamination by exogenous DNA. Finally, we performed de-duplication of merged reads with DeDup (53), which is optimized for merged paired-end sequencing data. This resulted in a final mean per-sample coverage of 9.7X.

We used the program MapDamage2.0 (54) to quantify damage patterns in the historical DNA. The fraction of C deamination, which leads to C-to-T substitutions, was low, at the first base ~2% on average across samples, barely inflated above the C-to-T substitution rate across the rest of the reads (Fig S3). Nonetheless, the fraction of C-to-T substitutions at the first base was positively correlated with the age of the samples ($r = 0.46$, $t = -5.31$, $p = 5.94\text{e-}07$; Fig S3). We thus used MapDamage2.0 to rescale base-quality scores to take into account the patterns of DNA damage. We called SNPs with freebayes (v1.3.2; with the arguments --use-best-n-alleles 4, --report-monomorphic) in 100 kb regions in parallel across the genome, merged, and then filtered SNPs based on the relationship between QUAL and DP ($\text{QUAL/DP} > 30$). In total, this resulted in 14,139,333 SNPs before merging with our contemporary data and filtering on missing data.

Herbicide resistance alleles in herbarium samples were identified based on known locations of non-synonymous substitutions within ALS and EPSPS. Initially, two genotype calls from herbarium samples that predated the onset of ALS herbicide use in the 1950s, showed standing variation for resistance at ALS574 and ALS122: one individual heterozygous for Trp-574-Leu collected in 1930 from a sandy agricultural field in St. Louis, Missouri, USA (HB0973); and another individual heterozygous for Ala-122-Ser collected in 1895 from a corn field in Fayette, Ohio, USA (HB0914). Upon further inspection, read-level support for resistance alleles was low with the allelic-bias at these genotype calls being highly skewed (reference to alternate ratio = 1:9 and 2:18, respectively). Similarly, one individual collected in 1967 from the Bottom of Maumee River, Ohio (HB0977) was heterozygous for ALS122, but the alternate resistance allele had support at only one read (reference to alternate ratio = 1:7). We subsequently dropped these genotype calls from analyses of selection on herbicide resistance alleles through time. Relatedly, for both the set of 154 focal agricultural-alleles and ancestry informative SNPs used to call fine-scale ancestry across the genome, we investigated the potential for reference bias influencing our estimates of change through time. We calculated mean allelic bias (AB) for each set of alleles individually for each sample, and asked the extent to which it correlated with collection year (Figure S3). AB for either set of alleles was not significantly correlated with collection year (AB for agricultural alleles: $\beta = 3.987 \times 10^{-5}$, $p = 0.316$, $t = 0.7527$; AB for ancestry informative alleles: $\beta = -3.877 \times 10^{-5}$, $p = -1.882$, $t = 0.0626$).

Metrics of differentiation across Environments: CMH, F_{ST} , & XPEHH

We used the 7,262,599 genome-wide high-quality SNPs called from contemporary agricultural-natural paired populations (n=187 individuals total from 17 pairs of populations, 34 populations in total) from (24) (Fig 1). Previously, these data had been only used for genome-wide PCA and faststructure based individual-level ancestry estimates. To make use of our paired sampling design, we used plink (55) to perform a Cochran–Mantel–Haenszel test, testing an (environment x SNP | pair) effect after applying a minor allele frequency cutoff of 0.01. We identified candidate agriculturally-adaptive genes based on the nearest gene (bedtools closest) to each LD-clumped, [FDR-corrected] q-value < 0.1 SNP. We found the *Arabidopsis thaliana* orthologues of our *A. tuberculatus* genes with orthofinder (56). For genes where orthofinder found no *A. tuberculatus* orthologue and in which our annotation identified no orthologue in closely related species based on gene expression data, we used blastn (57) to perform a conclusive search for similar genes across species.

Additionally, we used plink to calculate Weir and Cockerham's F_{ST} , both between all natural and agricultural samples, and between environments within each population pair, which we later averaged to obtain the mean pairwise F_{ST} . For calculation of F_{ST} at the EPSPS amplification, we recoded individuals as 0, 1, 2 based on copy number amplitude (<1.5, 1.5 < copies < 2.5, and >2.5, respectively). Briefly, EPSPS copy number was estimated in Kreiner (2019), through scaling coverage within the EPSPS gene by the genome-wide average. We used selscan (58) to calculate the cross-population extended haplotype homozygosity, after read-back and population-level phasing with Shapeit2 (59), both of which required knowledge of recombination rates, which we supplied in the format of our imputed LD-based map from (45).

Models of Migration-Selection Balance

Three resistance alleles showed significant differences in allele frequency across natural and agricultural environments (ALS574, EPSPSamp, and PPO210) based on a multiple regression approach (lm: genotype ~ pair + environment), reflecting differential selection pressures in the face of otherwise high rates of migration (as evidenced by the low genome-wide F_{ST}). Indeed, previous experimental work on costs on resistance has shown several of these herbicide resistance mutations to be associated with substantial costs: the ALS574 mutation has been associated with a 67% reduction in above ground biomass in *A. palmeri* (60) whereas the EPSPS amplification has been associated with a 25% reduction in dry biomass in *A. tuberculatus* (38) but is associated with no observed cost in *A. palmeri* (61). In the context of the experimental conditions and genotypes used in Wu et al., 2019 (62), no costs of the PPO210 deletion were found. However, genotypic and environmental heterogeneity is a major limitation of experimental approaches to assaying costs (63).

We take a model fitting approach that implicitly takes into account such heterogeneity by looking over a diverse set of genotypes, environments, and selective regimes. Specifically, we fit a two-patch, two allele model of migration-selection balance to estimate the relative magnitude of migration and selection across environment types. In each patch, we first assume that the life cycle starts at the adult stage, followed by migration and then selection among the juveniles to the next census among adults:

$$\begin{aligned}x_S^* &= (1 - m_A)x_S + m_A y_S, x_R^* = (1 - m_A)x_R + m_A y_R \\y_S^* &= (1 - m_N)y_S + m_N x_S, y_R^* = (1 - m_N)y_R + m_N x_R\end{aligned}$$

where m_N and m_A represent immigration rates into natural and agricultural sites, respectively; x_S^* and x_R^* represent the frequency of the susceptible and resistant allele in agricultural environments after migration; and y_S^* and y_R^* represent the frequency of the susceptible and resistant allele in natural environments after migration. Assuming random mating, the frequencies of resistant (in agricultural, x_R' ; in natural, y_R') and susceptible alleles (in agricultural, x_S' ; in natural, y_S') after selection are proportional to:

$$\begin{aligned}x_S' &= \frac{x_S^* (x_S^* W_{SS} + x_R^* W_{SR})}{x_S^* (x_S^* W_{SS} + x_R^* W_{SR}) + x_R^* (x_R^* W_{RR} + x_S^* W_{SR})}, \\x_R' &= \frac{x_R^* (x_R^* W_{RR} + x_S^* W_{SR})}{x_S^* (x_S^* W_{SS} + x_R^* W_{SR}) + x_R^* (x_R^* W_{RR} + x_S^* W_{SR})} \\y_S' &= \frac{y_S^* (y_S^* V_{SS} + y_R^* V_{SR})}{y_S^* (y_S^* V_{SS} + y_R^* V_{SR}) + y_R^* (y_R^* V_{RR} + y_S^* V_{SR})}, \\y_R' &= \frac{y_R^* (y_R^* V_{RR} + y_S^* V_{SR})}{y_S^* (y_S^* V_{SS} + y_R^* V_{SR}) + y_R^* (y_R^* V_{RR} + y_S^* V_{SR})}\end{aligned}$$

Where W and V reflect the average fitness of each genotype in agricultural and natural environments, respectively. Assuming additivity with s_N measuring the selective cost of the resistant allele in natural environments ($V_{RR} = 1 - s_N, V_{RS} = 1 - s_N/2, V_{SS} = 1$) and s_A measuring the selective benefit of the resistant allele in agricultural environments ($W_{RR} = 1 + s_A, W_{RS} = 1 + s_A/2, W_{SS} = 1$) and assuming that migration at the loci is much weaker than selection ($m \ll s$), a given pair of populations is expected to approach a steady state, where:

$$\frac{s_A}{m_A} = \frac{2(y_R - x_R)}{y_S y_R} \text{ in agricultural patches and } \frac{s_N}{m_N} = \frac{2(x_S - y_S)}{x_S x_R} \text{ in natural patches}$$

While it is not possible to solve for selection directly in the absence of data on migration rates, these formulae allow us to estimate the strength of divergence by inferring the strength of selection relative to migration in natural ($\frac{s_N}{m_N}$) and agricultural ($\frac{s_A}{m_A}$)

environments, as presented in **Table S3**. The ratio of these metrics gives the ratio of the cost faced per migrant that has arrived in natural environments versus the benefit per migrant that has arrived in agricultural environments, assuming that the pair of populations is near equilibrium. We note that the approach to migration-selection balance occurs exponentially at a rate proportional to the selection coefficient (when $m \ll s \ll 1$) and so should occur rapidly at sites under strong selection (**Supplemental Index 1**).

Logistic models of temporal allele frequency change

We used CMH outliers from the contemporary paired population scan to investigate patterns of agricultural-allele frequency change over the last two centuries. We were interested in tracking independent allele frequency trajectories, so from the 403 SNPs with CMH p-values that exceeded 10% FDR correction ($p < 6 \times 10^{-6}$), we performed a subsequent clumping step, effectively retaining a set of largely unlinked SNPs (**Fig S11**) that represent the most significant SNP in a particular region. Average LD across SNPs was 0.043, with only four pairs of SNPs showing high pairwise LD ($r^2 > 0.4$) with another SNP. All of these four SNP pairs are found on separate chromosomes from the SNP with which it has high LD, suggesting the correlation is not driven by linked selection (alternatively, genome-assembly or polygenic adaptation [such as in (43, 64)] may drive such a signal). Specifically, we used plink --clump, to find the most significant hit genome-wide, scan 1 Mb around it, and exclude any SNP from the resulting output that is in $r^2 > 0.25$ with the focal SNP. This algorithm is repeated until all SNPs passing the genome-wide significance threshold have been clumped. This resulted in 251 loci that on average showed a 17.9% allele frequency difference between extant agricultural and natural environments. Because some of the alternate alleles across these loci were more frequent in natural environments, we redefined the alleles based on which one was more common in agricultural compared to natural sites.

We then found the intersection of these agriculture-associated alleles, identified in our contemporary paired collections, with the historical, filtered SNPs from the herbarium sequence data. 154 loci were present in the historical samples with the same reference/alternate allele combinations. Because the definition of agriculture-associated alleles depend on their relative frequency across environment types, such alleles represent both reference (91/154) and alternate (63/154) bases. We extracted a matrix of 0, 0.5, 1 values, representing the frequency of the agricultural allele for each locus within each individual, for samples from both our contemporary and historical collections. Combining these individual agricultural allele frequencies at each locus across historical and contemporary datasets, we then performed a logistic regression in R (glm function, family="binomial") of genotype on collection year, separately on samples from either natural or agricultural environments. From each logistic regression, we extracted the logit-transformed slope, p-value, and standard error, as well as the predicted value (allele frequency) at 1870 and 2018, representing the minimum sample year and maximum sample year. The slope gives an estimate of the selection coefficient, s (specifically, slope

= $s/2$) where s is the difference in fitness between the two homozygotes and the division by two comes from using a diploid model. Specifically, with homozygote fitness of $1+s$ and heterozygote fitness of $\sqrt{1+s} \sim 1+s/2$, measured relative to the wildtype homozygote, the allele frequency over time has a generalized logistic form:

$$p(t) = \frac{p_0 e^{st/2}}{1 - p_0 + p_0 e^{st/2}}$$

where p_0 is the allele frequency at time (t) 0. While we have samples dating back to 1828, we constrained this analysis to samples collected after 1870, as the density of samples before then is low ($n=4$), with no representation of samples from agricultural environments.

The total allele frequency change at each locus was calculated by taking the difference between the predicted frequency of the allele in 2018 and 1870. We merged the output of these locus-specific logistic regressions in agricultural environments, with both SNP and haplotype-based statistics from these same individuals to identify contemporary correlates of the magnitude of allele frequency change and selection through time. Specifically, we examined how well contemporary recombination rate, XPEHH, CMH p -value, number of SNPs in linkage ($r^2 > 0.25$) with the focal SNP ($< 1\text{Mb}$; i.e., number of SNPs in a clump), and distance between linked SNPs, explained both the total allele frequency change and the estimated strength of selection (**Fig S6**).

We also performed a separate set of analyses, where a logistic regression was used to analyze the trajectory of all agricultural alleles or known herbicide resistance alleles at once, first across samples from natural environments and then for samples from agricultural and disturbed environments ('genotype ~ year + locus'; **Fig 3C, D**). We further partitioned samples in each environment to those that predate or are subsequent to the 1960s, to infer the importance of the intensification of agriculture and herbicides in shaping the strength of selection on contemporary agricultural loci. For each of the four logistic regressions ran on these partitioned sets of data, the slope of the year term represents a joint estimate of the strength of selection for agricultural alleles, between 1870-1960 or 1960-2018, in natural or agricultural environments. We refer to this joint estimate of selection at multiple loci as \tilde{s} .

To test whether a comparison of selection before and after the 1960's was statistically supported, we also compared our full model analyzing temporal signatures of allele frequency change between 1870-1960 to one that fits either two or three logistic regression lines between that time frame (i.e., a segmented logistic regression). A segmented logistic regression with two breakpoints provides the best fit to our data, compared to a model with either one or no breakpoints (two-break segmented AIC=54360.55, one-break segmented AIC =54437.66, non-segmented AIC=54444.67), and converges on 1913 and 1961 breakpoints, the later supporting a priori hypotheses and

our interest in interrogating signals before and after the start of the Green Revolution in 1960 (**Fig 3C**).

We designed a randomization test based on observed allele frequency changes across the genome to obtain an expected distribution under null processes (drift, migration, selection, and demographic change). In particular, we were interested in quantifying the potential bias in higher frequency agricultural alleles having the leeway to change more through time, as compared to a set of lower frequency alleles. We thus randomly sampled 154 loci from our contemporary collections (the same number as our observed clumped and historically matched set of agricultural alleles), 1000x across the genome, exactly matching the frequency distribution observed for extant agricultural alleles. This randomization was done independently in each environment, such that the alleles sampled to match the extant agricultural-allele frequency distribution in agricultural environments in one iteration were different from the alleles sampled to match the frequency distribution in natural environments (**Fig S4**). To account for the ascertainment bias in our set of putatively agriculturally adaptive alleles—alleles that show the greatest excess of allele frequency in agricultural compared to natural environments—we further constrained these randomizations to alleles across the genome which were at greater frequency in agricultural than in natural environments (which may reflect either the reference or alternate allele). In each of the 1000 randomizations within each environment, we then performed the same analyses as above: matching these alleles in our historical samples, producing a matrix of genotype data for both contemporary and historical sets, and performing a logistic regression for each locus, as well as logistic regression on all loci at once, for either samples from natural or agricultural environments, and for those that either preceded or were subsequent to 1960. For the 1000x randomizations within agricultural and natural environments, we then computed the 2.75 and 97.25% quantiles (“null 95% interquantile range”) of the statistics of interest (total allele frequency change and selection coefficients) to compare against our observed values. Note that these null expectations implicitly account for changing ancestry through time, as genome-wide genotypes from individuals spanning our temporal sampling produce the expectation of allele frequency change.

We performed forward-time simulations in SLIM (v3.7.1) to validate the robustness of our space-time herbarium sampling approach for inference of the strength of selection for a set of alleles. On a genomic background of length 100kb, with a recombination rate scaled to approximately that of *Arabidopsis thaliana* (4×10^{-6}), we started by evolving additive mutations (with a mutation rate of 5×10^{-6}) neutrally for 2000 generations in 5000 individuals. After this time period, we imposed an environmental shift which results in those once neutral mutations become beneficial [with an exponential distribution of fitness effects centered on $s=0.1$]. This represents selection on standing genetic variation, and potentially, any new mutations that arise after the onset of selection). After this environmental shift, we start our temporal sampling following the same temporal distribution and total sample size used in our manuscript (i.e $t = 0, 5, 6, 7, 10, 10, 12$

... 141, representing years sampled after 1870, $n = 104$ [removing four individuals from < 1870), with individuals randomly sampled across 2D space. From these simulations, we find our temporal and spatial historical sampling approach is able to provide an accurate estimate of s for a set of alleles. On average, the correlation coefficient between estimated s and true s using the method described above for 500 simulations was 0.61 (SE=0.067). The accuracy of this method will depend on the N (sequenced sample size), s (distribution of true selection coefficients) and N_e (species-wide) at hand.

Maximum likelihood estimate of selection

For known biallelic herbicide resistance alleles (excluding only the complex EPSPS amplification), we were particularly interested in individual estimates of selection on each allele over time. We used a maximum likelihood approach to estimate the strength of selection for each resistance allele between 1960-2018, along with a 95% credibility interval using profile likelihood. Summing overall years (t), the log-likelihood of observing the data is given by the binomial sampling formula describing the chance of observing the number of resistant (n_R) and susceptible alleles (n_S) in any given year:

$$\ln(L) = \sum_t (n_R \cdot \ln(\frac{p_0 e^{st/2}}{1 - p_0 + p_0 e^{st/2}}) + n_S \cdot \ln(\frac{1 - p_0}{1 - p_0 + p_0 e^{st/2}}))$$

where p_0 represents the frequency of the allele when $t = 0$ (defined as the present for ease of computation) and s represents the strength of selection (see logistic allele frequency trajectory equation above), both of which are unknown and estimated by maximizing the likelihood. Because many of the resistant alleles were only observed in contemporary samples, selection must be sufficiently strong on recent timescales to explain this rise, but the maximum strength of selection cannot be determined (the likelihood surface becomes flat). We thus only present the 95% confidence interval in the text (i.e., those values of s for which the $\ln(L)$ falls within $\chi^2_{[0.05]}/2$ of the maximum likelihood). We implemented this algorithm in R, using the mle2 function implemented within the bblme package in R.

Ancestry inference

For genome-wide ancestry inference, we merged filtered SNPs from herbarium samples with high-quality SNP sets from (24) ($n=187$, collections from 2018) and (45) ($n=162$, collections from 2015), resulting in 457 individuals and representing all resequenced *A. tuberculatus* whole genomes (n of SNPs = 1,269,007). We used faststructure (46) to infer individual-level ancestry, taking the proportion of an individual's assignment to a grouping at $K=2$ to represent either var. *rudis* or var. *tuberculatus* ancestry. An individual's proportion of var. *rudis* ancestry was then analyzed in a multivariate regression that tested how well var. *rudis* ancestry was explained by longitude, latitude, environment (natural or agricultural), timespan (1800-1920 [$n=39$], 1920-1980 [$n=44$],

1920-2020 [n=374]), a two-way timespan by longitude interaction, a two-way timespan by state interaction, and a three-way timespan by environment by longitude interaction (Individual ancestry assignment ~ longitude + latitude + environment + timespan + timespan:longitude + timespan:state + timespan:environment:longitude)

We also used plink to perform a principal-component analysis of merged SNPs from just herbarium samples (**Fig S12**) and all 457 samples jointly (**Fig S13**).

We were interested in the distribution of var. *rudis* ancestry across the genome, and so used LAMP (65) to assign ancestry to SNPs, based on two reference populations homogenous for either var. *rudis* or var. *tuberculatus* ancestry (Kansas and Ontario Natural Populations, respectively; (45)). Ancestry informative SNPs were those with an $F_{ST} > 0.40$ (2x the mean genome-wide ancestry differentiation between varieties, in these two populations) between these reference populations and that were also in common between datasets (<20% of samples with missing data) after merging historical sequences with the contemporary paired sequence data (24). Since LAMP requires recombination rate information, we also imputed the LD-based genetic map from (45) to the ancestry-informative SNPs to get genetic distance between each. Finally, we performed the LAMP analysis, one population at a time, one scaffold at a time. After merging SNP-wise ancestry assignments across scaffolds, we calculated the mean, 5%, and 95% quantile of var. *rudis* ancestry in 100 kb regions for each population, and eventually, each environment (**Fig S10**).

To understand the relationship between ancestry, agricultural selection, and genomic architecture, we performed a multiple regression to quantify drivers of fine-scale ancestry across the genome. We regressed the individual proportion of var. *rudis* ancestry in 100 kb windows across the genome against gene density, recombination rate, scaffold, environment, average CMH score, average XPEHH (difference in extended haplotype homozygosity across environments), the interaction between environment and average CMH score in each window, and the interaction between environment and the mean XPEHH in each window (100kb mean ancestry ~ scaffold + mean gene density + mean recomb + mean xpehh:env + mean cmh:env + env). The least squares effect of environment on ancestry was taken to calculate the average difference in ancestry between agricultural and natural environments.

Tables S1 to S5

Table S1. GO Enrichment results for the top 0.1% CMH outliers (n=7264 SNPs, 1650 orthologous genes in *Arabidopsis thaliana*).

GO biological process complete	Expected Alleles	Fold Enrichment	Bonferroni corrected p-value
anatomical structure formation involved in morphogenesis	15.41	2.4	0.0161
anatomical structure development	322.07	1.3	7.59E-05
developmental process	352.41	1.31	2.19E-06
post-embryonic development	138.32	1.46	7.06E-04
multicellular organism development	264.29	1.32	2.47E-04
multicellular organismal process	284.88	1.3	6.92E-04
reproductive structure development	121.64	1.45	9.21E-03
reproductive system development	121.76	1.45	9.33E-03
system development	223.18	1.33	3.46E-03
reproductive process	160.77	1.38	9.11E-03
reproduction	162.39	1.37	1.52E-02
response to light stimulus	123.57	1.42	2.14E-02
response to radiation	126.22	1.46	3.33E-03
response to abiotic stimulus	249.49	1.35	6.75E-05
response to stimulus	562.59	1.24	1.55E-07
organic cyclic compound metabolic process	184.54	1.32	4.77E-02
organic substance metabolic process	589.08	1.19	1.37E-04
metabolic process	649.69	1.2	6.38E-07
regulation of cellular metabolic process	190.98	1.32	3.73E-02
regulation of cellular process	375.46	1.23	5.85E-03
regulation of biological process	456.6	1.21	2.30E-03
biological regulation	498.73	1.22	9.43E-05
regulation of metabolic process	237.21	1.29	2.52E-02
cellular response to stimulus	234.8	1.3	1.16E-02
cellular process	919.46	1.2	1.11E-15
response to chemical	308.77	1.29	2.83E-04
cellular metabolic process	573	1.22	7.54E-07
nitrogen compound metabolic process	423.67	1.21	8.41E-03
primary metabolic process	487.78	1.17	4.62E-02

Table S2. Gene and orthologue information for the 50 SNPs with the most significant CMH p-values, sorted by Scaffold and then CMH p-value. AMATA=*Amaranthus*

1054 *tuberculatus*, AT=*Arabidopsis thaliana*.
1055

Scaffold	Position	CMH p-value	AMATA gene	AT gene	Orthologue	Blastn
1	59264411	6.08E-10	2592	NA	Na	Nuclear Fusion Defective 4-like
1	55158523	3.29E-09	2285	At4g34215	SGNH-hydrolase	
1	54510509	8.91E-09	2244	NA	NA	NA
1	12324718	1.93E-07	825	AT5G09550.1	Guanosine nucleotide diphosphate dissociation inhibitor (GDI)	
1	64789405	2.39E-07	3031	AT4G38380.4	Protein DETOXIFICATION 452C chloroplastic (DTX45)	
10	15265237	7.25E-08	22183	NA	NA	NA
10	26222541	1.03E-07	22540	AT3G29385.1	Dentin sialophosphoprotein-like protein	
10	5374087	2.74E-07	21789	NA	N NA	NA
11	24079642	8.55E-11	25990	AT5G63460.1	Lower temperature 1	
11	24078348	3.09E-10	25990	AT5G63460.1	Lower temperature 1	
11	24086055	1.10E-09	25990	AT5G63460.1	Lower temperature 1	
11	24006946	2.18E-09	25984	AT5G14220.4	PPO2	
11	24062979	2.36E-09	25989	AT5G50380.1	Exocyst complex component EXO70B1	
11	24080739	4.33E-09	25990	AT5G63460.1	Lower temperature 1	
11	32783081	7.71E-09	26623	NA	NA	
11	24048769	1.30E-08	25988	AT4G14110.1	COP9 signalosome complex subunit 8 (CSN8)	
11	24047019	4.13E-08	25988	AT4G14110.1	COP9 signalosome complex subunit 8 (CSN8)	
11	24083434	4.40E-08	25990	AT5G63460.1	Lower temperature 1	
11	24070607	4.79E-08	25989	AT5G50380.1	Exocyst complex component EXO70B1	
11	26024805	1.35E-07	26127	AT1G75125.1	Plastid transcriptionally active protein	
11	25369807	1.47E-07	26088	AT5G39610.1	Nucleobase-ascorbate transporter 6 (NAC6)	
11	24021382	1.69E-07	25985	AT5G16550.1	Ldap interacting protein	
11	24024155	1.69E-07	25985	AT5G16550.2	Ldap interacting protein	
11	24048722	2.07E-07	25988	AT4G14110.1	Constitutive photomorphogenic 9	
11	24046969	2.55E-07	25988	AT4G14110.1	Constitutive photomorphogenic 9	
12	29335314	7.69E-10	24987	ATMG00310.1	Orf154	
12	29335422	3.09E-09	24987	ATMG00310.1	Orf154	
12	29327164	3.31E-09	24987	ATMG00310.1	Orf154	
12	29343299	1.81E-08	24987	ATMG00310.1	Orf154	
12	29336458	3.50E-08	24987	ATMG00310.1	Orf154	
12	29333763	5.83E-08	24987	ATMG00310.1	Orf154	
12	11427671	7.91E-08	24182	NA	NA	PPX2L
12	29328119	1.21E-07	24987	ATMG00310.1	Orf154	
12	11429925	2.10E-07	24182	NA	NA	PPX2L
12	29333575	2.30E-07	24987	ATMG00310.1	Orf154	
12	29333622	2.30E-07	24987	ATMG00310.2	Orf155	
13	35715956	8.71E-09	19321	NA	Calmodulin (Physarum polycephalum OX%253D5791)	
13	38847060	6.31E-08	19605	NA	NA	WIP2-like protein
13	26858220	8.73E-08	18867	NA	NA	NA
13	33084574	1.93E-07	19117	AT4G14310.2	KIN14B-interacting protein	
13	41600578	2.63E-07	19862	AT3G24160.1	Putative type 1 membrane protein	
2	53114550	8.86E-08	5599	NA	NA	NA
2	10688517	9.38E-08	3997	AT3G09630.1	Suppressor of acaulis 56 (sac56)	
3	4797458	8.95E-09	6345	NA	NA	ATHB13
3	1072396	9.09E-09	5998	AT1G23820.1	Spermidine synthase 1	
3	1072448	8.96E-08	5998	AT1G23820.1	Spermidine synthase 1	
3	16438213	1.27E-07	7059	AT1G10150.1	Carbohydrate-binding protein	
3	5632229	1.80E-07	6414	AT4G09650.1	Atp synthase delta-subunit gene (atpd)	
6	18669007	1.54E-07	15047	AT4G35830.1	Aconitase 1 (ACO1)	
8	15398786	1.13E-08	20978	AT3G14310.1	Pectin methylesterase 3	

1056
1057
1058 **Table S3.** Selection-migration differentiation statistics for 8 resistance alleles, along with
1059 estimates of selection estimated by logistic regression of the allele frequency through
1060 time. Ag, agricultural sites; Nat, natural sites. Cost and benefit estimates shown here for

the additive ($h=0.5$) case. s (1960-2018) represents the maximum likelihood estimate of selection from the binomial sampling equation of allele frequency change based on a diploid model of selection, and we provide the associated 95% credible interval.

	Ag Freq	Nat Freq	Ag Benefit (s/m _s)	Nat Cost (s/m _s)	Cost/Ben	s (1960-2018)	95% CI of s
PPOdel	0.334	0.0464	2.58582	12.9997	5.027303	1.16	0.194, ∞
EPSPSamp	0.496	0.236	2.08013	2.88402	1.386461	NA	NA
EPSPS106	0.127	0.087	0.721559	1.00716	NA	1.12	0.106, ∞
ALS122	0.0301	0	NA	NA	NA	-0.01	$-\infty$, ∞
ALS197	0.0132	0.0169	NA	NA	NA	0.286	$-\infty$, ∞
ALS574	0.337	0.191	1.30689	1.88974	1.445982	0.09	0.088, 0.334
ALS376	0.0824	0.0358	1.23264	2.70001	NA	0.59	0.046, ∞
ALS653	0.0596	0.0627	-0.11062	-0.105498	NA	0.55	0.058, ∞

Table S4. The top 15 loci with the strongest evidence of temporal selection between 1970 and 2018.

s	s p-value	AF s(SE) change	scaf	position	AMATA annotated gene	AT orthologue	AT gene name
0.106	4.680E-04	0.030 0.846	Scaffold_11	26068182	AMATA_chromosomes_26131	NA	NA*
0.081	1.081E-04	0.021 0.823	Scaffold_2	10755264	AMATA_chromosomes_03999	Subtilase family protein	AT5G58840
0.057	2.382E-03	0.019 0.512	Scaffold_10	22995135	AMATA_chromosomes_22407	phosphotyrosyl phosphatase activator (PTPA family protein)	AT4G08960
0.052	8.211E-03	0.020 0.402	Scaffold_11	26024805	AMATA_chromosomes_26127	plastid transcriptionally active protein	AT1G75125*
0.052	6.084E-05	0.013 0.646	Scaffold_3	14213167	AMATA_chromosomes_06976	WRKY DNA-binding protein 13	AT4G39410
0.047	2.549E-07	0.009 0.783	Scaffold_10	36863790	AMATA_chromosomes_23250	hypothetical protein	AT1G36320
0.046	1.272E-01	0.030 0.162	Scaffold_3	49332690	AMATA_chromosomes_08117	NA	NA
0.045	2.889E-05	0.011 0.677	Scaffold_6	18669007	AMATA_chromosomes_15047	ACO1	AT4G35830
0.043	8.557E-05	0.011 0.599	Scaffold_12	21792253	AMATA_chromosomes_24760	NA	NA
0.043	4.601E-08	0.008 0.888	Scaffold_3	5632229	AMATA_chromosomes_06414	ATPD (F-type H ⁺ -transporting ATPase subunit delta)	AT4G09650
0.036	8.069E-06	0.008 0.666	Scaffold_12	5658420	AMATA_chromosomes_23853	NA	NA
0.033	4.729E-07	0.007 0.831	Scaffold_10	20690917	AMATA_chromosomes_22321	CCB2 (chaperone DUF2930)	AT5G52110
0.032	1.755E-07	0.006 0.819	Scaffold_10	16005835	AMATA_chromosomes_22202	NA	NA
0.032	3.939E-05	0.008 0.708	Scaffold_10	24312710	AMATA_chromosomes_22452	BPA4 (RNA-binding RRM/RBD/RNP motifs family protein, AT1G14340)	AT1G14340
0.031	5.175E-06	0.007 0.764	Scaffold_2	17891465	AMATA_chromosomes_04209	NA	NA

* ~2 Mb from PPO

Table S5. Metadata on herbarium collections.

Sample	Herbarium	Year	State	County/Locality	Description	Nat/Ag/Dist	Lat	Long	Catalog #
--------	-----------	------	-------	-----------------	-------------	-------------	-----	------	-----------

HBO900	INHS	1876	Illinois	Oquawka	Banks of the Mississippi	Nat	40.900098	-90.991298	1
HBO901	INHS	1870	Illinois	Kankakee	Wet Banks	Nat	41.154318	-87.919365	2
HBO902	INHS	1875	Illinois	Oquawka	Banks of the Mississippi	Nat	40.900098	-90.991298	3
HBO903	INHS	1897	Illinois	Warrenville	Mudflats	Nat	41.823199	-88.174393	6
HBO904	INHS	1892	Illinois	Chicago	Waste Ground ("Exposition Building")	Dist	41.779452	-87.61641	7 (429)
HBO907	INHS	1897	Illinois	Chicago	Dumping ground, Brighton Park	Dist	41.818787	-87.706608	10
HBO908	INHS	1952	Illinois	Fithian, Vermilion County	Along railroad	Dist	40.114645	-87.875056	11 (56279)
HBO909	INHS	1946	Illinois	Gardenplain, Whiteside County	Peat soil in potato field, "L.C. Anderson Farm"	Ag	41.782572	-90.138152	12 (19934)
HBO910	INHS	1948	Illinois	W of Antioch, Lake County	Disturbed soil	Dist	42.481444	-88.157622	13 (32479)
HBO911	INHS	1947	Illinois	W of Gillespie, Macoupin County	Corn field	Ag	39.127901	-89.860508	14 (22536)
HBO912	INHS	2005	Illinois	Minooka Rd & Route I-80, Minooka	Disturbed moist cropland margin near sable creek	Ag	41.457917	-88.308444	15 (242814)
HBO913	INHS	2000	Illinois	Cooperstown, Brown County	Former marsh in partly filled obow, mostly used as corn fields	Ag	39.959059	-90.611708	16 (205271)
HBO914	MBDH	1895	Ohio	Fulton Co.	Cornfield along the new river improvement on the prairie	Ag	41.67333333	84.32694444	357
HBO915	MBDH	1903	Ontario	Essex Co.	NA	NA	41.772246	-82.79184	265
HBO916	MBDH	1955	Ohio	Greene Co.	Front lawn of Campus house	Dist	39.82083333	84.01944444	292
HBO917	MBDH	1956	Ohio	Mercer Co.	Roadside, edge of soybean field	Ag	40.67861111	84.51861111	197
HBO918	MBDH	1991	Ohio	Putnam Co.	Weedy ground alongside Blanchard River	Nat	41.03944444	84.15694444	253
HBO919	IUH	1898	Indiana	Lake	on ballast (railroad bed)	Dist	41.602259	-87.25837	IND-0088703
HBO920	IUH	1941	Indiana	Vanderburgh	cultivated ground	Ag	37.870283	-87.634147	IND-0088729
HBO921	IUH	1941	Indiana	Vanderburgh	field north of river slough	Ag	37.979365	-87.544518	IND-0088730
HBO922	IUH	1952	Indiana	Johnson	Low cornfield	Ag	39.482726	-86.019624	IND-0088699
HBO923	IUH	2007	Indiana	Vigo	Mesic loam plain fallow cropland with successional weeds	Ag	39.43257	-87.380135	IND-0088738
HBO924	KUMH	1897	Missouri	Jackson, Courtney	Common along river	Nat	39.15556	-94.39333	176647
HBO925	KUMH	1913	Kansas	Doniphan,	Mesophytic oat field.	Ag	39.813187	-95.160615	43812
HBO926	KUMH	1913	Kansas	Doniphan,	Mesophytic oat field.	Ag	39.813187	-95.160615	43965
HBO927	KUMH	1949	Kansas	Shawnee, Lake Shawnee	Dry grassland.	Nat	39.000784	-95.626093	43811
HBO928	KUMH	1940	Kansas	Douglas, Lawrence	Field.	Ag	38.9365	-95.22391	44000
HBO929	KUMH	1970	Kansas	Chautauqua, Peru	Low, cultivated field. Gumbo soil.	Ag	37.09524	-96.07752	43956
HBO930	KUMH	1973	Kansas	Allen, Elsmore	Roadside right of way along field. Weedy, good soil.	Ag	37.79382	-95.16832	43987
HBO931	KUMH	1981	Kansas	Doniphan, Denton	Edge of cultivated field.	Ag	39.70289	-95.30739	43933
HBO932	KUMH	1994	Kansas	Labette, Parsons	Disturbed roadside along bean field and adjacent woodlands to the S. (scattered pop in field)	Ag	37.29416	-95.210223	111589
HBO933	ROM	1891	Ontario	NA	Leading to the H null Cemetery	Dist	43.892294	-81.312444	447
HBO934	ROM	1889	Ontario	Wingham	Alluvial soil (wet soil)	Nat	43.89161	-81.312795	189975
HBO935	ROM	1880	Ontario	London	Fields	Ag	42.954827	-81.234897	188334
HBO936	ROM	1891	Ontario	Leasselman	Alluvium along the Nation River	Nat	45.319337	-75.093578	438

HBO937	ROM	1880	Ontario	North Branch, London	Low River Flats	Nat	43.04267	-81.175264	441
HBO938	ROM	1940	Ontario	New Durham, Brant Co	Edge of Field	Ag	43.04956	-80.523938	129548
HBO939	ROM	1960	Ontario	Dunnville, Haldimand Co	Wasteground by Lake Erie	Dist	42.86879	-79.617923	159479
HBO940	ROM	1950	Ontario	Kent Co	Wet sand at Rankin creek near Mitchell Bay	Nat	42.48877	-82.413605	80.118
HBO941	ROM	1960	Ontario	Grenville Co, ON	Muddy shore of South Nation River	Nat	44.828922	-75.554629	134207
HBO942	ROM	1986	Ontario	Walpole Island	Disturbed forest/tall grass prairie - swampy	Nat	42.568369	-82.504545	TRT00029148
HBO943	ROM	1991	Ontario	Louth Twp., Niagara RM	W Shoreline of Jordan Marsh	Nat	43.174444	-79.375015	246184
HBO944	ROM	1985	Ontario	Ottawa-Carleton	Silty wet sand in dried-up pond in old pasture	Dist	45.274525	-76.088545	234833
HBO945	ROM	1988	Ontario	Wasaga Beach	Nottawasaga R. at Jack L.	Nat	44.485637	-79.99545	240977
HBO947	ROM	1997	Ontario	Brighton Tw., Northumberland Co	Sand pile, N shore of Lake Ontario	Nat	43.997787	-77.729332	256250
HBO948	ROM	1990	Ontario	Wingham	Riverbanks	Nat	43.89161	-81.312795	27813
HBO949	ROM	1880	Ontario	N.B. London	River flat	Nat	43.083152	-81.166767	85.246
HBO950	UMH	2001	Michigan	Lenawee Co	Open roadside at edge of cornfield, S side of Lime Creek Rd, w of Rogers Hwy	Ag	41.766065	-84.227971	1209687
HBO951	UMH	1909	Michigan	near Port Huron	Invading cultivated fields as a weed, abundant	Ag	42.979577	-82.470627	1209704
HBO952	UMH	1897	Illinois	Warrenville	Mud flats	Nat	41.829751	-88.177826	1559076
HBO953	UMH	1883	Ohio	Cincinnati	NA	NA	39.136053	-84.502294	1207957
HBO954	UMH	1833	Ohio	North Bend, Cincinnati	Sandy beach of Ohio River	Nat	39.14757	-84.753428	1207929
HBO955	UMH	1932	Ontario	Little Current, Manitoulin Island	In open fields	Ag	45.966667	-81.933333	1208039
HBO956	UMH	1986	Ontario	Essex Co, Malden Twp	Big creek marsh	Nat	42.05088	-83.056715	1208029
HBO957	UMH	1946	Illinois	Sangamon Co	Woods	Nat	39.578464	-89.730027	1208025
HBO958	UMH	1989	Ontario	N Plantagenet Ip, Jessup's Falls (South Nation PP), Hwy 17 @ S Nation R	Rockshore protection and waste ground along river	Dist	45.559302	-75.064719	1207959
HBO959	UMH	1882	Illinois	Riverside	Gravelly, dry bed of Des Plaines River	Nat	41.826723	-87.82569	1559075
HBO961	UMH	1949	Illinois	Champaign Co	Mud and sand at bottom of a ditch	Dist	40.061911	-88.105443	1559082
HBO962	UMH	1993	Ontario	Middlesex Co, Lobo Twp,	Komoka Creek Swamp near Thames River, Edge of Thames	Nat	42.917996	-81.441417	1207956
HBO963	UMH	1995	Ontario	Niagara Regional Municipality, Niagara Falls Twp	Moist disturbed ground near railway tracks	Dist	43.06736	-79.084574	1208030
HBO964	MO	1877	Illinois	Saint Clair	Low places	Nat	38.55	-89.916667	1740835
HBO965	MO	1889	Missouri	St. Louis City	NA	NA	38.62975	-90.242434	1740859
HBO966	MO	1893	Illinois	Saint Clair	Low places	Nat	38.509011	-90.177817	1740847
HBO967	MO	1897	Illinois	Warrenville	Mudflats *note: same pop/date/collector as #93	Nat	41.829751	-88.177826	38973
HBO968	MO	1902	Illinois	Saint Clair	Wet plains in East St Louis	Nat	38.625	-90.16	1740833
HBO969	MO	1912	Missouri	St. Louis City	In open field	Ag	38.603097	-90.257021	778075
HBO960	MO	1919	Illinois	Pope	Muddy banks of Ohio River	Nat	37.364829	-88.482798	853159
HBO970	MO	1925	Illinois	Lake	Wet open ground, borders of tamarack swamp	Nat	42.370872	-88.121862	940825

HBO971	MO	1927	Missouri	St. Louis	Mo River Sand Bar	Nat	38.595548	-90.767735	2157288
					In moist ground near Sugar Loaf Station, about 2 miles south of Du Po				1026850
HBO972	MO	1927	Illinois	St. Clair		Dist	38.495758	-90.217877	
HBO973	MO	1930	Missouri	St. Louis	Sandy fields	Ag	38.715451	-90.48898	2157285
					Alluvial banks along Mississippi river, 6500 South St. Louis				1140474
HBO974	MO	1933	Missouri	St. Louis		Nat	38.572701	-90.229642	
					Moist thicket along Sangamon River, 15 miles west of Urbana				1579795
HBO975	MO	1940	Illinois	Champaign		Nat	40.119754	-88.498602	
HBO976	MO	1962	Illinois	Tazwell	Low River Bank	Nat	40.720818	-89.597212	1812554
					Bottom of Maumee River at SW corner of Maumee city Limits				6773122
HBO977	MO	1967	Ohio	Lucas		Nat	41.542549	-83.689433	
					Weedy mowed and cultivated fields and bulldozed areas				6113965
HBO978	MO	2005	Illinois	Madison		Ag	38.779167	-89.640556	
					Howell Island Conservation area, huge population, in large field next to hiking trail				6449615
HBO979	MO	2009	Missouri	St. Charles		Nat	38.665567	-90.70705	
					Dallas city public fishing access on the bank of the Mississippi River, and nearby railway tracks				6443667
HBO980	MO	2009	Illinois	Hancock		Nat	40.634567	-91.179467	
HBO981	MO	2010	Missouri	Montgomery	Loutre River	Nat	38.911389	-91.592778	6334467
					Roadside through floodplain with deep alluvial sandy loam				6341594
HBO982	MO	2011	Illinois	Randolph		Dist	37.923333	-89.893333	
					A common weed in low and cultivated ground				6773126
HBO983	MO	1919	Missouri	Jasper		Ag	37.204167	-94.344167	
HBO984	AAFC	1892	Ontario	Ottawa	NA	NA	45.289379	-75.737232	1001151662
					3 miles East, Wet Roadside				
HBO985	AAFC	1955	Ontario	Richmond, Carleton		Dist	45.19477	-75.78076	1151663
					Shoreline of Ottawa River, moist sandy gravelly soil				
HBO986	AAFC	1954	Ontario	Rockcliffe Park		Nat	45.457179	-75.676253	1151664
HBO987	AAFC	1921	Ontario	Ottawa	Lac Constane	Nat	47.387012	-77.283366	1151665
					1 mile N of York, Sand beach				
HBO988	AAFC	1951	Ontario	Haldimand County		Nat	43.035303	-79.897787	1151667
					East beach, moist sand beach				
HBO989	AAFC	1988	Ontario	Essex County		Nat	41.93464	-82.505179	1151668
					North shore or W End, Moist woods				
HBO990	AAFC	1998	Ontario	Essex County		Nat	41.683999	-82.682764	1151669
					Dried bed of the Raisin River at rapids				
HBO991	AAFC	1964	Ontario	Glengarry County		Nat	45.13414	-74.575361	1151671
					Along sandy beach, Between Mississippi River & McEwan Nay.				
HBO992	AAFC	1949	Ontario	Lanarck		Nat	45.046655	-76.230997	1151672
					High grass along tracks, Railyards north of the station				
HBO993	AAFC	1960	Ontario	Sarnia		Dist	42.957915	-82.393943	1151673
HBO994	AAFC	1937	Ontario	Ottawa	Shore line, Moira Lake	Nat	44.486839	-77.458612	1151674
					Muddy inundated shore of South Nation River				
HBO995	AAFC	1960	Ontario	Grenville County		Nat	44.951292	-75.483802	1151675
					Rocky Point Prov. Park, Dunville Twp.				
HBO997	AAFC	1988	Ontario	Hald-Norfolk County		Nat	42.847407	-79.555433	1154001
HBO998	AAFC	1958	Ontario	Stormont County	Railway tracks	Dist	44.988422	-74.996022	1151676
HBO999	AAFC	1938	Ontario	Pelee Island	NA	Nat	41.683999	-82.682764	1154003
HB1000	AAFC	1934	Ontario	Mitchell's Bay	Waste places	Dist	42.468738	-82.407807	1154004
					Edge of 1st Island below Gault				
HB1001	AAFC	1939	Ontario	Waterloo County		Nat	43.352835	-80.316045	1154005

HB1002	AAFC	1918	Ontario	NA	NA	NA	42.77177	-81.197887	1154008
HB1003	AAFC	1961	Ontario	Waterloo County	Wet Field beside Speed River	Ag	43.455939	-80.290772	1154009
HB1004	AAFC	1828	Ontario	Middlesex County	Thames River	Nat	42.959472	-81.309866	1154010
HB1005	AAFC	1828	Ontario	Middlesex County	Bank of the Thames	Nat	42.980389	-81.344198	1154011
HB1006	AAFC	1961	Ontario	Waterloo County	Wet Field beside Speed River	Ag	43.455939	-80.290772	1154012
HB1007	AAFC	1966	Ontario	Middlesex County	Muddy soil alongside creek	Nat	43.030996	-81.349254	1154014
HB1008	AAFC	1828	Ontario	Middlesex County	NA	NA	42.950068	-81.435938	1154013
HB1009	AAFC	1903	Ontario	NA	In boggy soil	Nat	43.892294	-81.312444	1151660
HB1010	INHS	1906	Illinois	Riverdale	Along railroad	Dist	41.640523	-87.626446	8 (2632)
HB1011	INHS	1894	Illinois	Wheaton	Roadside	Dist	41.864251	-88.103346	9 (267)

1079
1080
1081 Figures S1 to S13
1082
1083

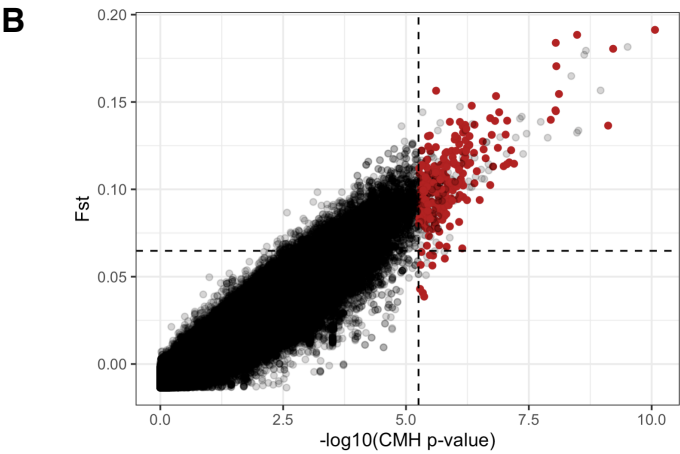
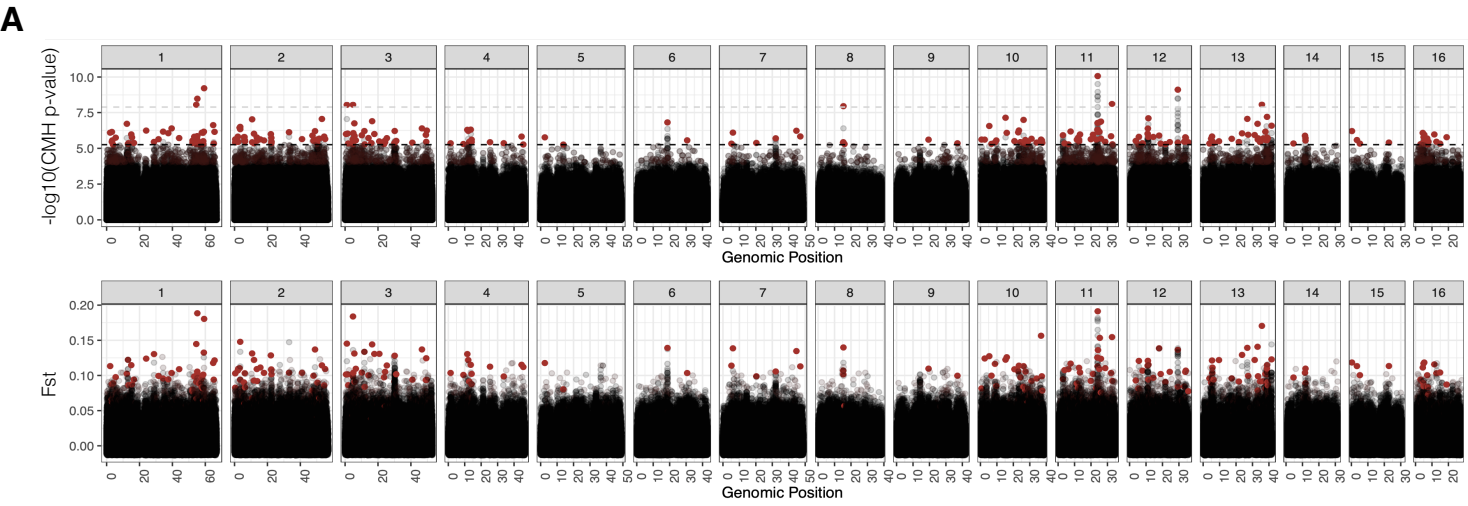


Fig S1. Strong congruency between results of a CMH genome-wide scan (assessing environmental differences stratifying for population pair) versus a between-environment F_{ST} genome-wide scan (differentiation among individuals pooled within natural environments and within agricultural environments). A) Two Manhattan plots showing the distribution of CMH $-\log_{10}(p\text{-values})$ [top] and F_{ST} values at SNPs across the genome. B) Between-environment F_{ST} is plotted against the CMH $-\log_{10}(p\text{-values})$, showing a strong correlation (Spearman's $\rho = 0.905$; Pearson's r between F_{ST} and CMH $\chi^2 = 0.957$). In both A and B, red dots indicate focal putative agriculturally adaptive SNPs as inferred from the CMH scan, based on showing the strongest significance in a given 1 Mb region.

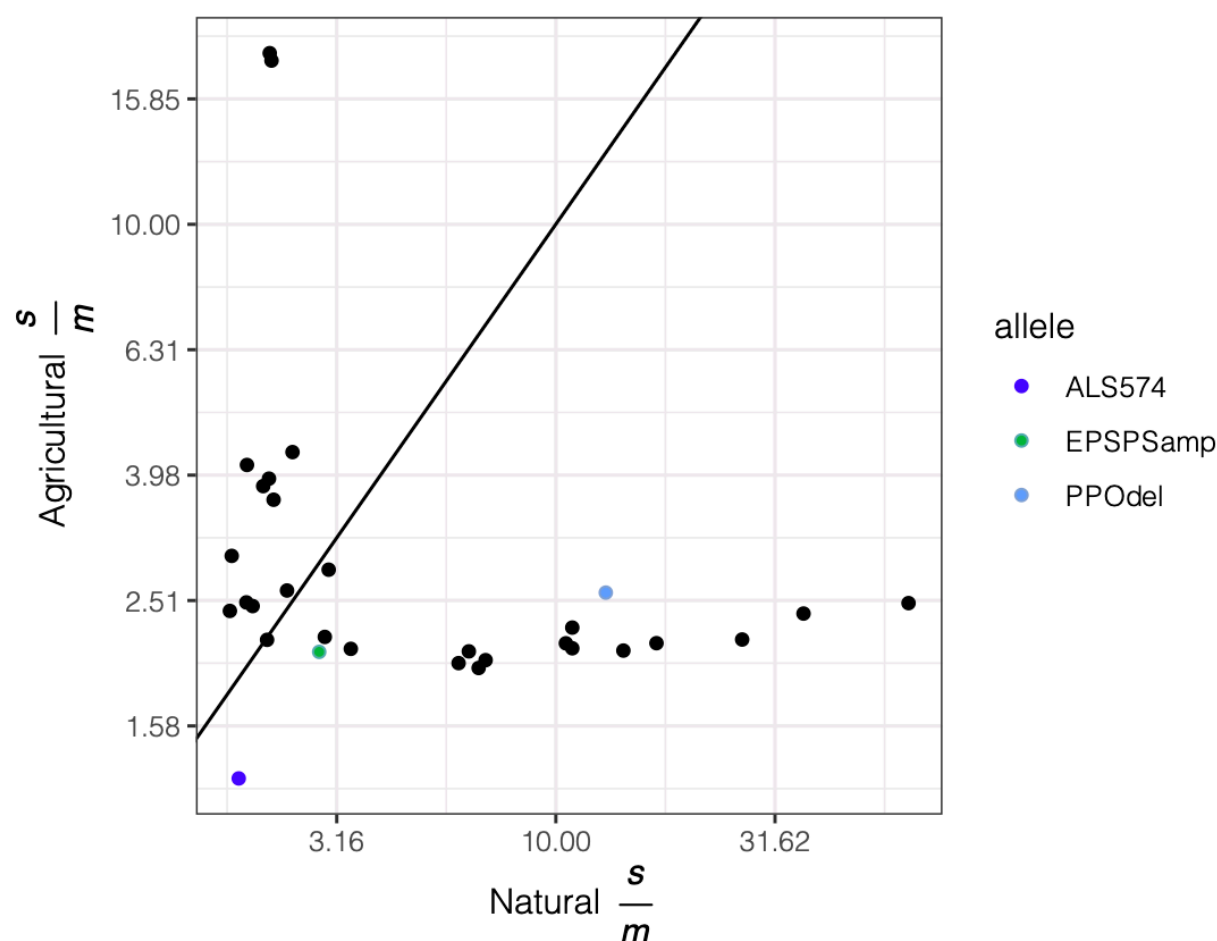


Fig S2. Agricultural $\frac{s}{m}$ (representing the migration scaled selective benefit) versus natural $\frac{s}{m}$ (representing the migration scaled selective cost) for the 30 independent loci with the most significant CMH scan hits, compared to the 3 common herbicide resistance alleles with significantly different allele frequencies among natural and agricultural environments. Diagonal line represents equal agricultural benefits compared to natural costs, scaled by migration.

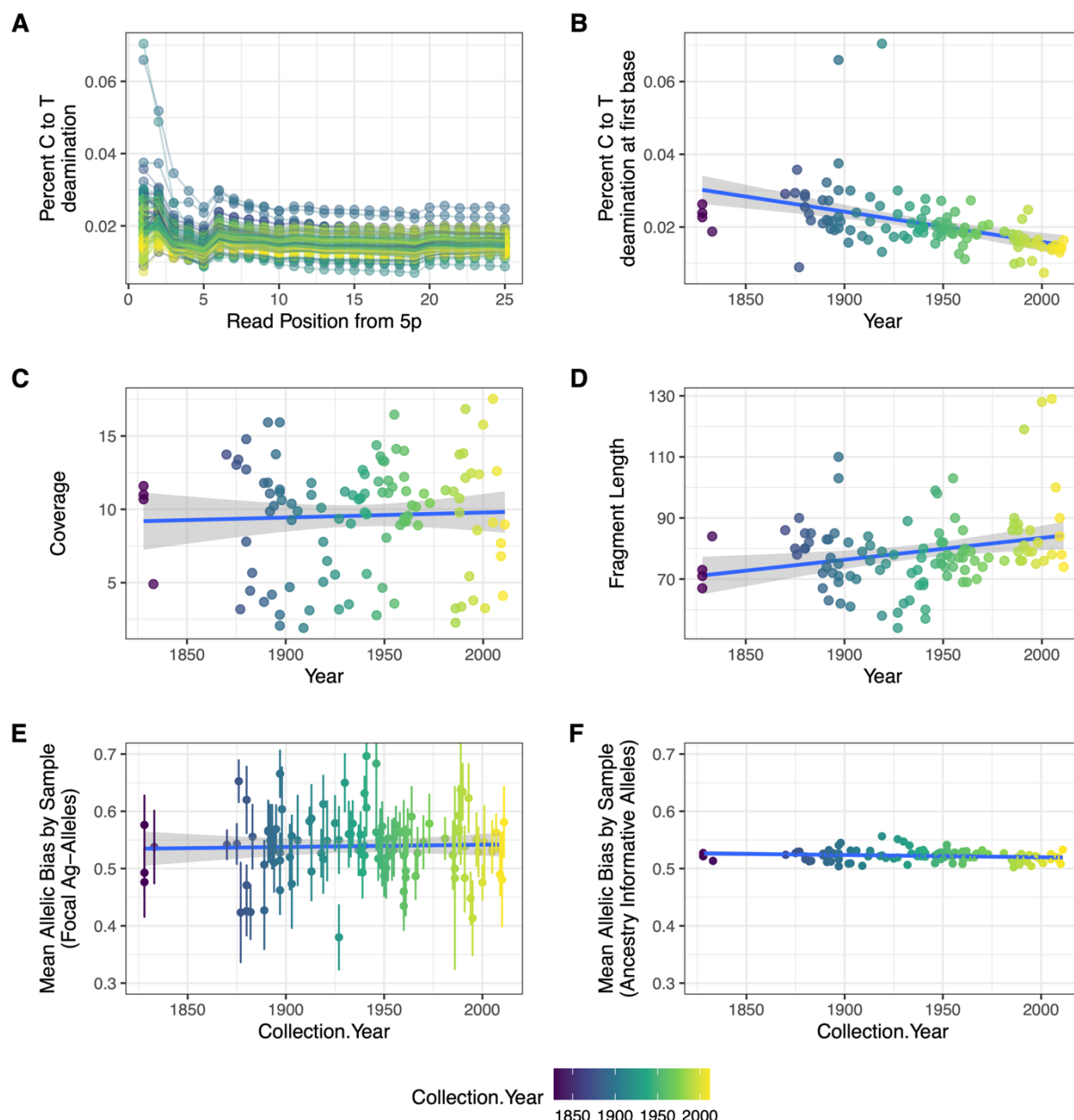


Fig S3. Percent C-to-T deamination by read position (A), along with the correlation of collection year with Percent C-to-T deamination at first base (B). C-D represent temporal correlates with genome-wide coverage (C), fragment length (D), mean allelic bias by sample for focal agriculture-associated alleles (E) and for ancestry informative alleles (F). For B-F, each dot represents sample-wise means for 108 sequenced herbarium specimens.

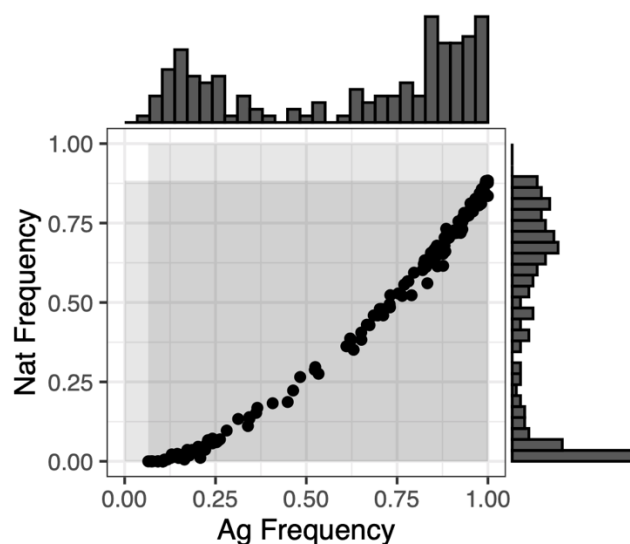


Fig S4. The distribution of frequencies for agriculturally adaptive alleles in agricultural samples along the x-axis, and in natural samples along the y-axis. Null distributions for an expectation of change in the frequency in our focal set of contemporary alleles was generated by producing randomized allele sets of the same size ($n=154$) matching the extant agricultural-allele frequency distributions shown here, first in natural environments (top histogram), and then in agricultural environments (right histogram).

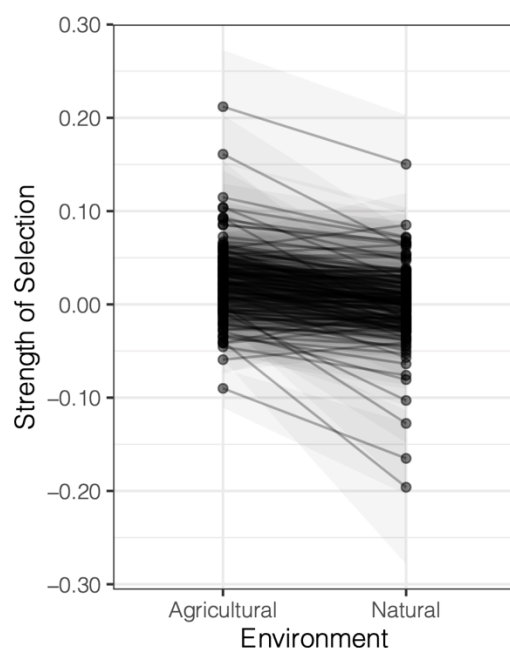


Fig S5. Inferred strength of selection on 154 agricultural alleles through time, in either agricultural or natural environments. Selection coefficients were extracted from logit-transformed logistic regressions of genotype on year, run separately for each locus in each environment. Gray ribbon for each locus represents the bounds of the standard error associated with the estimate of selection in each environment.

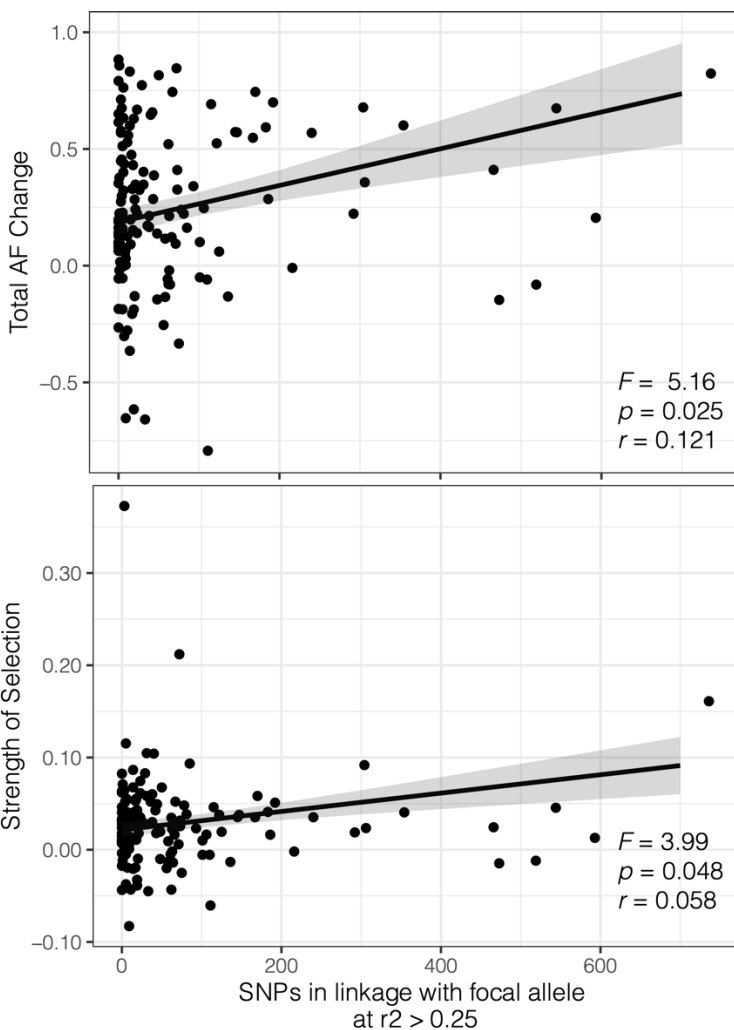


Fig S6. The association between contemporary patterns of linkage and selection and allele frequency change observed over the last 150 years across herbarium samples. Regression line shows the least square mean effect of contemporary linkage from a multiple regression analysis.

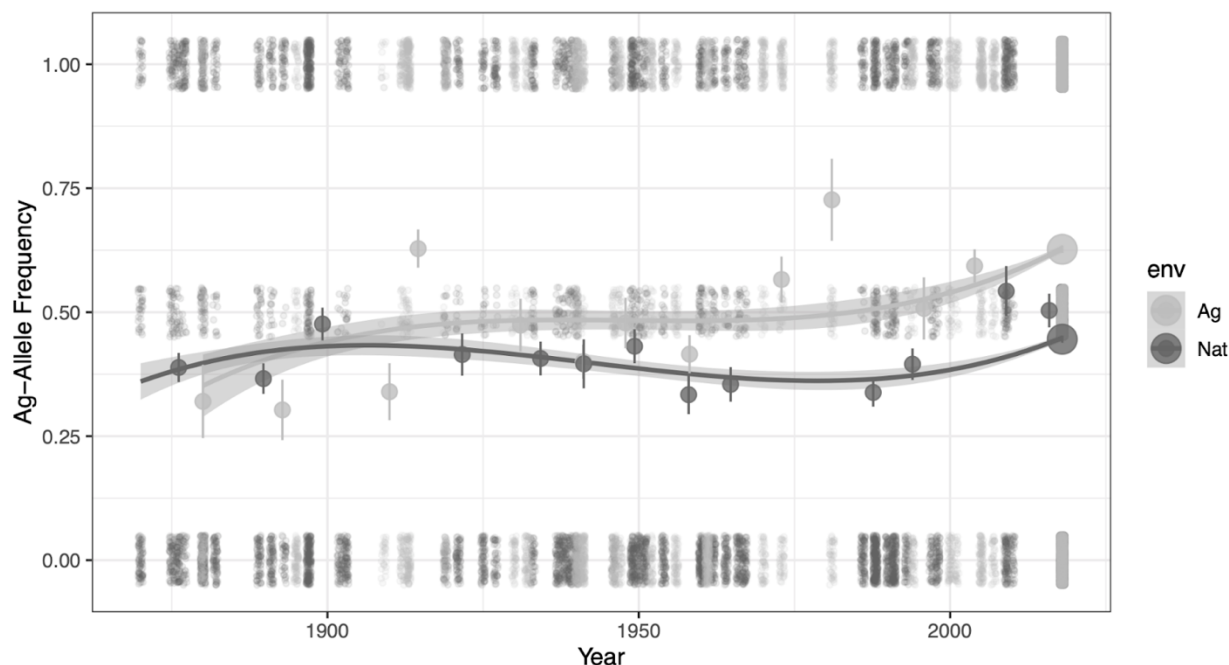


Fig S7. Cubic splines that illustrate the environment-specific frequency change of agricultural alleles through time since 1870. Gray ribbon denotes the 95% CI.

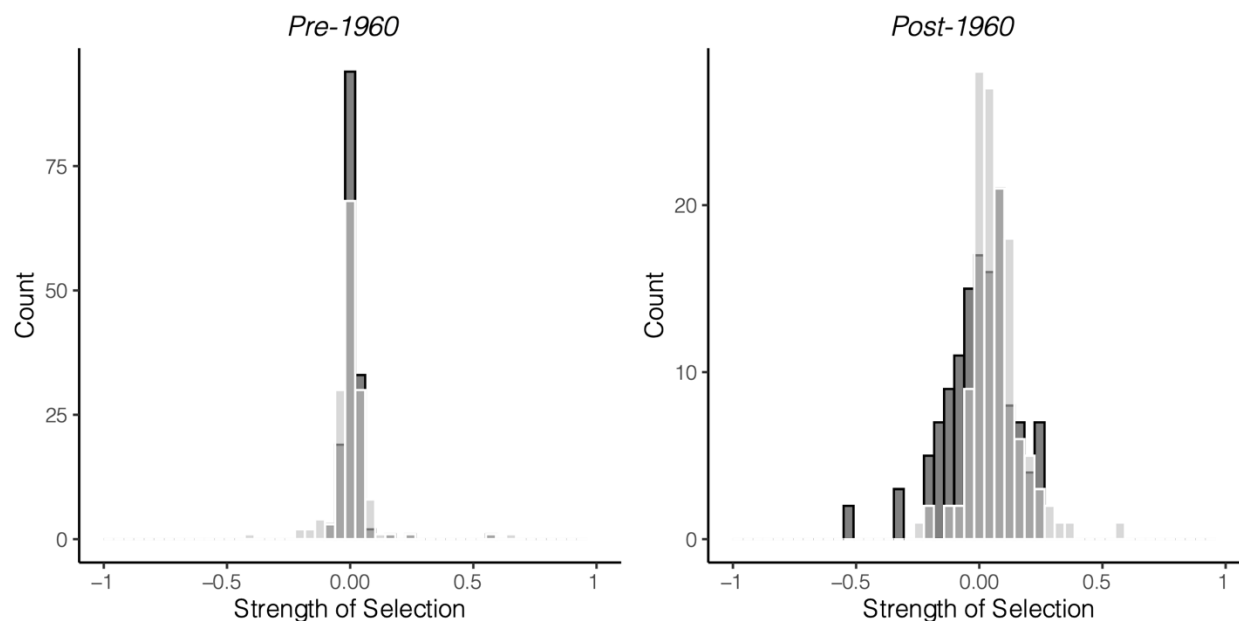


Fig S8. Logistic estimates of selection before (left) and after (right) the 1960s, the start of agricultural intensification, for agriculturally-associated alleles in natural (dark gray) versus agricultural and disturbed (light gray) environments.

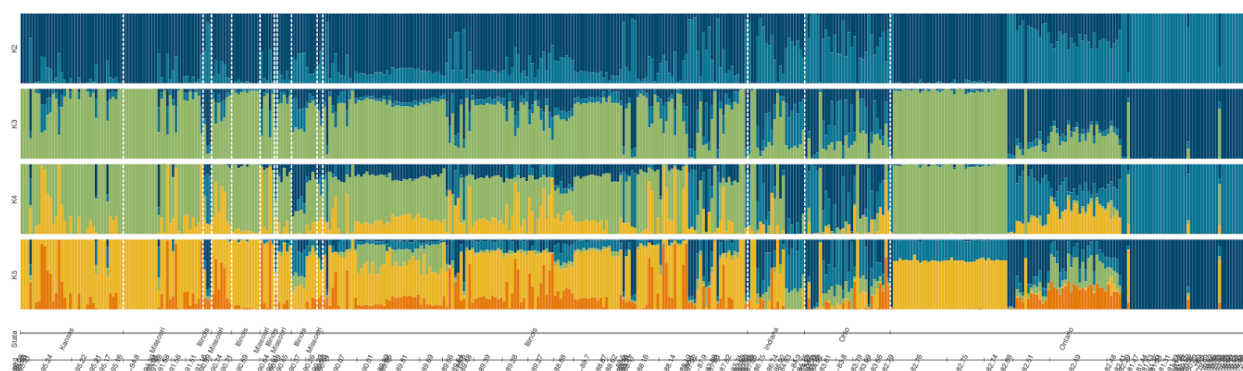


Fig S9. Longitudinal and state-wise patterns of ancestry across 457 *A. tuberculatus* individuals from contemporary and historical sampling, inferred from faststructure. Samples sorted by longitude, from west (left) to east (right). White dashed lines denote clusters of specimens sampled from different states and provinces across this longitudinal gradient. K=2 taken as var. *rudis* versus var. *tuberculatus* ancestry, as in (45).

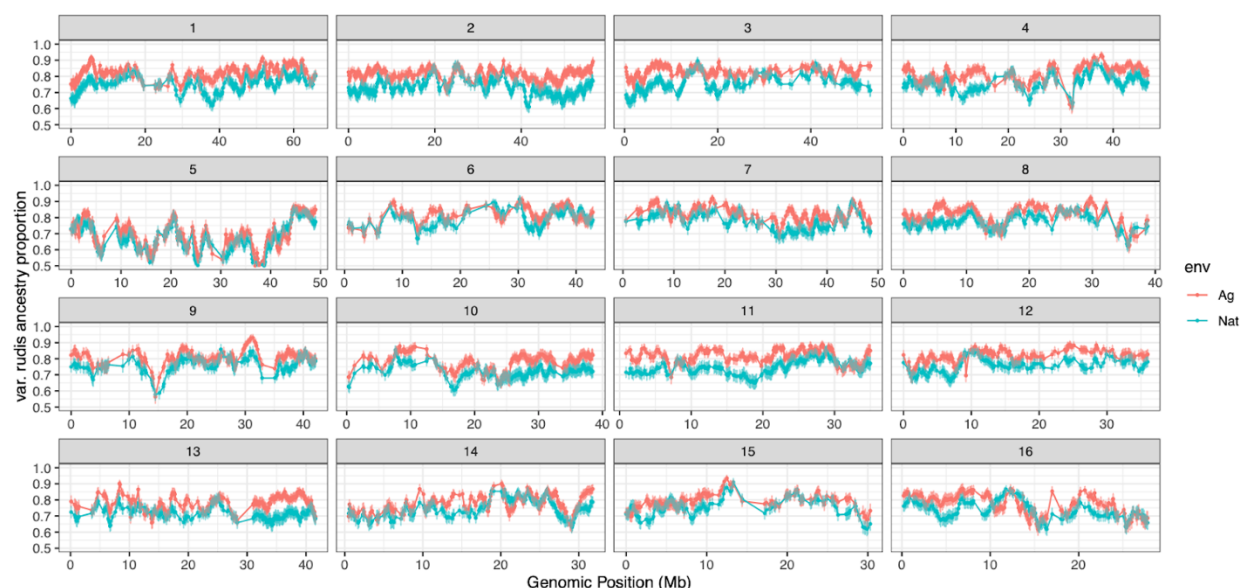
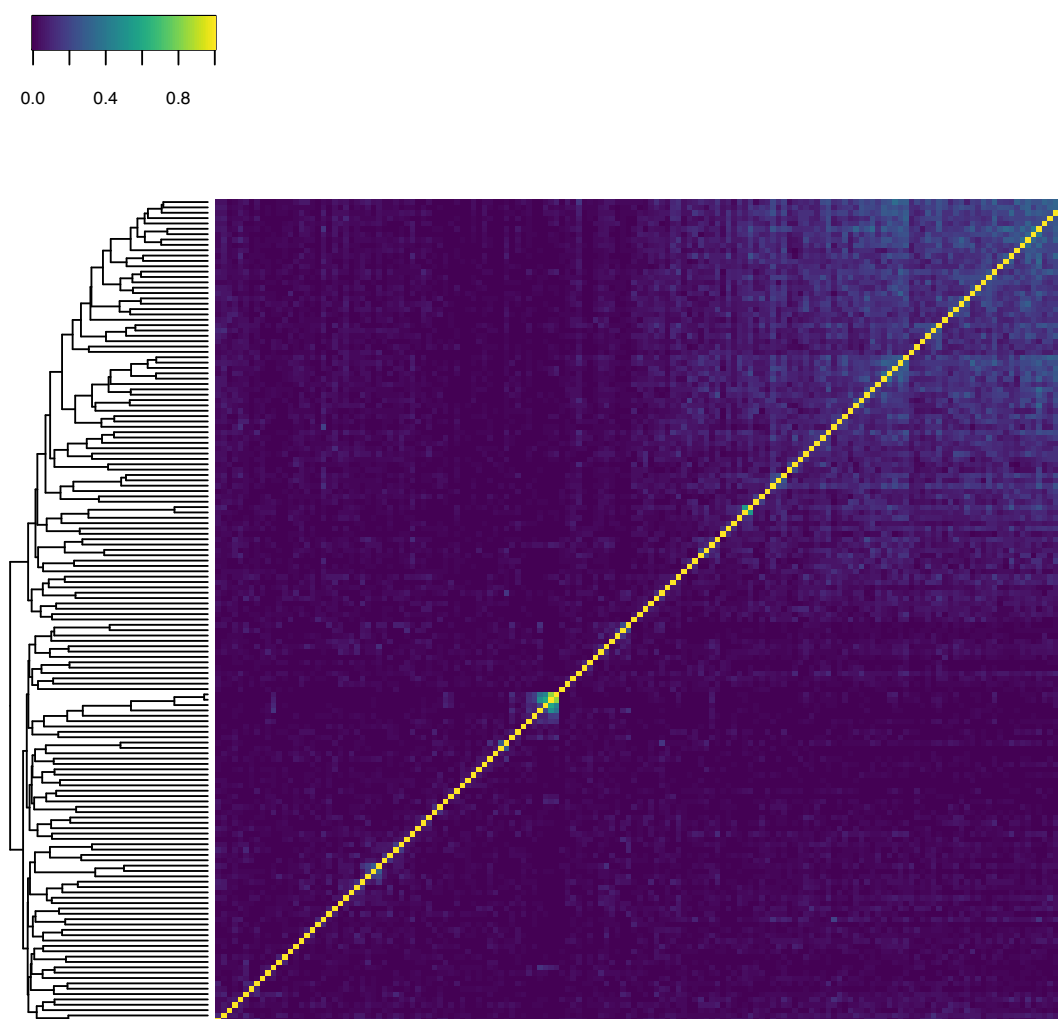


Fig S10. Excess of var. *rudis* ancestry in agricultural compared to natural environments, in 100 kb regions across the genome. Lines depict the mean ancestry across all populations within each environment, with error bars showing the mean 5th and 95th percentile of ancestry across populations. Fine-scale ancestry estimates were inferred with LAMP (65).

1161



1162
1163 **Fig S11.** Heatmap of r^2 values alongside a dendrogram of the 154 agriculturally
1164 associated SNPs identified through CMH tests across paired contemporary natural-
1165 agricultural samples, illustrating independence among focal LD-clumped CMH outliers.
1166
1167
1168
1169

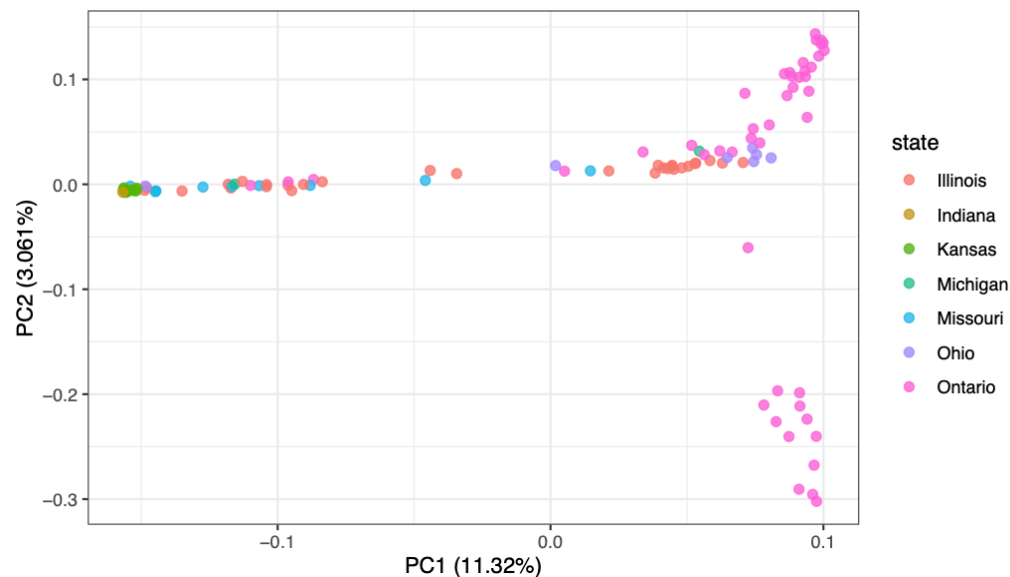


Fig S12. PCA of herbarium samples, colored by state/province.

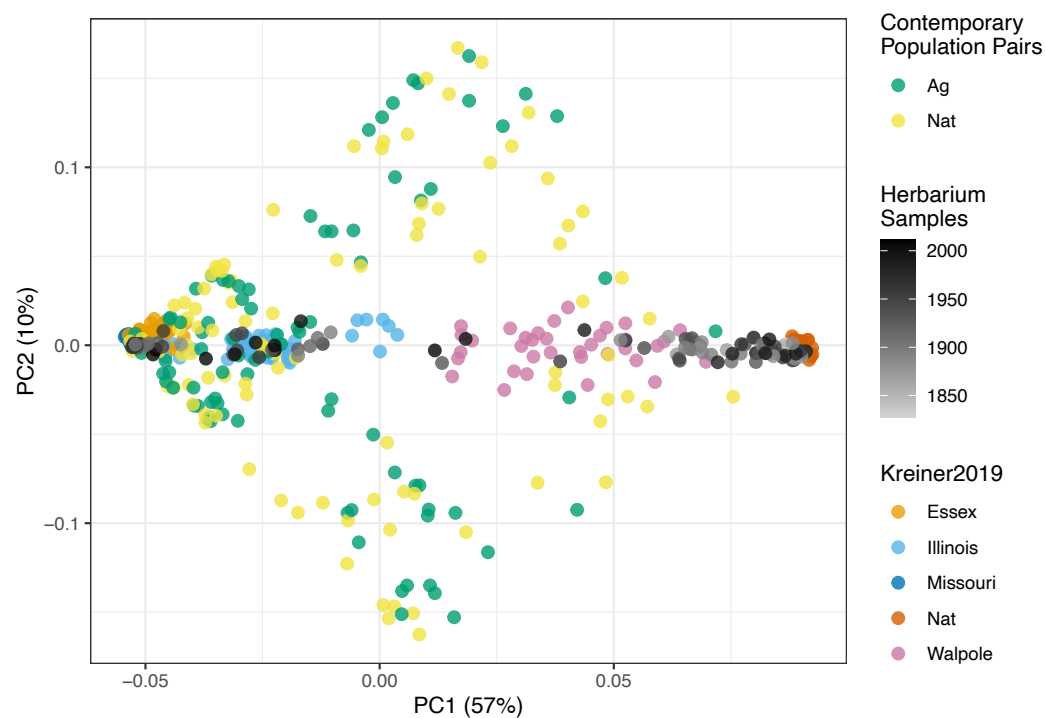


Fig S13. PCA of 457 *A. tuberculatus* specimens, including 108 herbarium samples along with contemporary paired populations (24) (n=187) and 21 populations from 5 geographic regions (45) (n=162).

Figure Captions

Fig 1. Sequenced waterhemp collections through space and time. **A)** Map of 17 contemporary paired natural-agricultural populations [n=187, collected and sequenced in Kreiner et al., 2021 (24)], along with 108 novel sequenced herbarium specimens dating back to 1828 collected across three environment types (Ag=Agricultural, Nat=Natural, Dist=Disturbed). **B)** Distribution of sequenced herbarium samples through time.

Fig 2. Signals of contemporary agricultural adaptation, gene flow, and antagonistic selection across the genome in *A. tuberculatus*. **A)** Results from Cochran–Mantel–Haenszel (CMH) tests for SNPs with consistent differentiation among environments across contemporary natural-agricultural population pairs. A 10% FDR threshold is indicated by the lower dashed horizontal black line, while the Bonferroni corrected p-value < 0.1 cutoff is shown by the upper dashed horizontal gray line. Red points indicate focal adaptive SNPs after aggregating linked variation ($r^2 > 0.25$ within 1 Mb). Candidate agriculturally adaptive genes for peaks that are significant at a 10% FDR threshold shown. **B)** CMH results from the scaffold containing the most significant CMH p-value, corresponding to variants linked to the PPO210 deletion conferring herbicide resistance and to the nearby herbicide-targeted gene *ALS*. **C)** Distribution of F_{ST} values between all agricultural and natural samples for ~3 million genome-wide SNPs (minor allele frequency > 0.05). Vertical lines indicate F_{ST} values for the 10 candidate genes named in A. **D)** Population-level frequencies of six common herbicide resistance alleles across geographically paired agricultural and natural habitats sampled in 2018 (pairs connected by horizontal lines). The first four columns are nonsynonymous variants in *ALS* and *EPSPS*, followed by *EPSPSamp* (a 10 Mb-scale amplification that includes *EPSPS*), and lastly, an in-frame single-codon deletion in *PPO*. Estimates of per-migrant natural cost: agricultural benefit ratio (C:B) is shown in the top right corner for the three resistance alleles with a significant (*) allele frequencies differences (AFA) across environment types.

Fig 3. Genomic signatures of agricultural adaptation through time. **A)** Agricultural allele frequency trajectories for each 154 focal SNPs, in agricultural and disturbed habitats (left), and natural habitats (right). Trajectories colored by the empirical quantile of frequency change in agricultural and disturbed habitats. Transparent lines indicate those with non-significant evidence of selection at $\alpha=0.05$ after FDR=10% correction. **B)** The distribution of selective strengths on agricultural alleles in natural (dark gray) and agricultural/disturbed (light gray) habitats between 1870 and 2018. **C)** Environment-specific agricultural allele frequency trajectories, before and after the start of agricultural intensification in 1960 (vertical dashed line). Large circles represent moving averages (over both loci and individuals) of allele frequencies, whereas dots represent raw genotype data for each locus and sample from which the allele frequency trajectory is estimated. Cropland use per capita in North America data from (1), rescaled by use in 1600, to reflect intensity of agricultural practices. **D)** The trajectory of alleles at known herbicide resistance loci through time, fit by logistic regression for each of the biallelic resistance alleles present in our contemporary data (excluding *EPSPSamp* with its complex allelic structure). Dots represent genotypes for each historical and contemporary sample at each herbicide resistance locus. 95% credible interval of the maximum likelihood estimate of selection between 1960-2018 provided in the legend for each resistance allele.

Fig 4. Temporal shifts in the distribution of var. *rudis* ancestry have facilitated polygenic agricultural adaptation. **A)** Longitudinal clines in individual-level var. *rudis* ancestry over three timespans, illustrating the expansion of var. *rudis* ancestry eastwards over the last two centuries. **B)** The distribution of individual-level var. *rudis* ancestry by state and through time, illustrating state-specific changes in ancestry. Vertical lines represent first, second, and third quantiles of ancestry within each timespan and state. Timespans indicated in (A). No individuals were collected from Kansas between 1828-1920. **C)** Increasing sorting of individual-level var. *rudis* ancestry into agricultural environments on contemporary timescales. **D)** Environment-specific metrics of selection (CMH p-value and cross-population extended haplotype homozygosity (XPEHH)) across the genome in 100 kb windows positively correlate with var. *rudis* ancestry in agricultural, but not natural habitats (XPEHH by Environment: $F=9.34$, $p=0.002$; CMH by Environment: $F=99.70$, $p < 10^{-16}$).